further selected by blastcidin and used within 14 days. shRNA sequences are described in the Supporting Information Methods.

Cell viability and apoptosis analyses. For the cell proliferation assay, 5000 cells were plated in a 96-well flat bottom plate with RPMI1640 medium supplemented with 1% FCS. After 1–3 days culture, cell numbers were evaluated using Cell Counting kit-8 (Dojindo, Kumamoto, Japan). The apoptosis cell was determined using PE Annexin V/7-AAD stainings (BD Pharmingen, San Jose, CA, USA). Detection of apoptotic cells was performed using FACSCalibur (Becton, Dickinson, Franklin Lakes, NJ, USA). Primary ATL cells were defined using sequential gating based on a Forward scatter/Side Scatter (FSC/SSC) pattern and a CD4-positive population (anti-CD4-FITC; BD Pharmingen). Collected data were analyzed using FlowJo software (Tree Star, Ashland, OR, USA).

Results

Epigenetic abnormalities in *EVC* regulation in ATL. We have determined the gene expression signature of ATL tumor cells by conducting massive microarrays.[5] The gene expression profiles from 52 ATL patients and 21 healthy donors identified a large number of specific gene upregulations in ATL cells. Among these, the genes encoding EVC1 and EVC2 were strikingly overexpressed in ATL patient samples, which had a relationship to disease progression (Fig. 1a,b). These genes are located in an identical chromosome *4p16*, under a bi-directional promoter (Fig. 1c), and their expressions have shown a strong positive correlation (Fig. 1d). The qRT-PCR revealed that the median of the *EVC1* mRNA level in ATL was 90.9-fold higher than that of normal CD4+ T-cells (Fig. 1e). Specificity of tumor-associated EVC expression was confirmed using the dataset from CADM1 versus CD7 plot subpopulation samples.[25] CADM1 expression and CD7 loss have recently been identified as highly sensitive molecular markers of HTLV-1-infected cells. *EVC1* and *EVC2* were significantly expressed in the CADM1+/CD7− tumorous population (Fig. 1f). The HTLV-1-infected and ATL-derived cells showed higher levels of *EVC1* mRNA compared with those in other leukemia and lymphoma cell lines and those of healthy PBMC (Fig. 1g). The MT-2 and HUT102 cells, which highly express HTLV-1 genes, showed high *EVC1* mRNA levels similar to those in ATL-derived cells.

Looking at the tumor-associated epigenetic reprogramming that was frequently observed in ATL,[5,6] we analyzed the epigenetic status of the *EVC* locus to clarify the possible

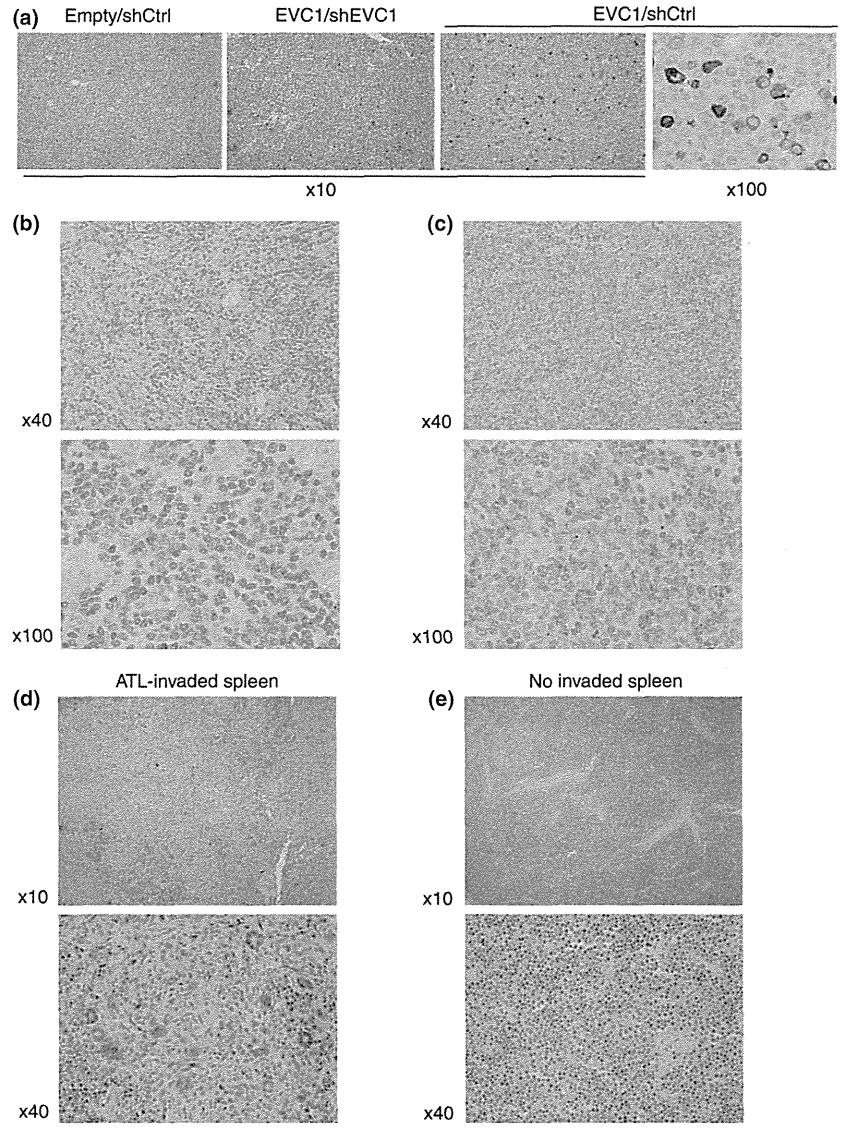

Fig. 4. EVC1 expression in ATL cells. (a–e) Immunohistochemistry-based EVC1 protein detection in paraffin-embedded samples: 293T transfected with the indicated plasmids (a), primary ATL lymph node (b, c, representative data are shown) and spleen from mice engrafted with primary ATL cells (d, tumor invasive, $n = 3$; e, non-invasive). These samples were stained with anti-EVC1 antibody and hematoxylin.

involvement of epigenetic variation in *EVC* deregulation. There were two typical CpG islands in the *EVC* locus whose transcription may be tightly regulated by the gain of CpG methylation (Fig. 2a). However, bisulfite sequencing revealed that DNA methylation was not acquired in normal lymphocytes, as well as in the primary ATL sample (Fig. 2b). CpG hypermethylation within the *EVC* locus was found only in Jurkat cells where the *EVC* expression was nearly undetectable (Fig. 1g). Instead, treatment with epigenetic drugs, particularly a histone deacetylase (HDAC) inhibitor tricostatin A (TSA), reactivated the *EVC* transcription in Jurkat cells, suggesting that histone modifications such as acetylation were involved in *EVC* regulation (Fig. 2c). To further address the epigenetic implication, we performed ChIP assays to assess the possible contribution of histone modification in *EVC* upregulation. The ATL cell lines showed significant accumulation (log-scale) of histone H3 acetylation (H3Ac) and H3K4 trimethylation (H3K4me3), which have been recognized generally as positive transcription marks around the transcription start site region of both *EVC1* and *EVC2* (Fig. 2d). Treatment with a pan-histone acetylase inhibitor, anacardic acid, reduced *EVC* transcription in ATL cell lines (Fig. 2e). Interestingly, H3K27me3, which has been implicated as a poor prognostic marker in ATL,[5,26] was decreased at the *EVC* locus in ATL cells. We confirmed directly the epigenetic reprogramming at the *EVC* locus in primary ATL samples (Fig. 2f). In summary, it appeared that the acquisition of active histone modifications and the reciprocal disappearance of H3K27me3 contributed to aberrant EVC transcription.

Role of HTLV-1 Tax in *EVC* transcription. Next we addressed whether Tax could participate in the deregulated *EVC1* transcription. Although Tax expression did not influence the *EVC1* mRNA levels in 293T cells at complete growth conditions, Tax activated *EVC1* transcription in a dose-dependent manner in serum-starved conditions (Fig. 3a). A NF-κB activation-defected Tax mutant, M22,[27] showed similar *EVC1* induction, suggesting that *EVC1* transcriptional activation was independent from NF-κB activation. Indeed, the pharmacological inhibition of NF-κB activity failed to prevent *EVC* transcription in ATL cell lines (data not shown). Meanwhile, Tax induced transcription of *Sonic hedgehog* (*Shh*), which encodes the HH activation ligand, in a NF-κB-dependent manner (Fig. 3b). The experimental condition was validated by the evaluation of *PTHrP*, which has been known to be a Tax and NF-κB-targeted gene. HTLV-1 *HBZ* did not affect *EVC* transcription (Supporting Information Fig. S1).

We examined the possible relationship between Tax and histone modifications. For this purpose, we established lentiviral vectors inducing stable Tax expression in Jurkat cells. More than 80% of transduction efficiencies were achieved in all tested cells. Tax induced transcription of *EVC1* and *EVC2*, as well as the HH target gene *PTCH1* (Fig. 3c). Interestingly, the Tax C29A mutant, which was unable to localize in the nucleus,[28] failed to induce *EVC*, suggesting that *EVC* induction was directly caused by the nuclear-localized Tax. A ChIP assay revealed that the Tax wild type, but not the C29A mutant, directly accumulated H3K4me3 and H3Ac in the *EVC* locus (Fig. 3d). Thus, Tax appeared to, at least partially, induce *EVC* expression through epigenetic reprogramming.

EVC1 expression in primary ATL cell. We performed immunohistochemistry (IHC) with a commercially available antibody that recognized EVC1. First, we stained paraffin-embedded 293T cells transduced with the EVC1-expressing plasmid to test the antibody specificity. Strong positivity was detected in the plasmid-transduced sample but not in samples with untreated or concomitantly treated with shRNA targeting *EVC1* (Fig. 4a). Using this antibody we investigated EVC1 expression in several aggressive ATL cases. Most ATL cases showed stable EVC1 positivity (7/8, 87.5%; two representatives in Fig. 4b,c). We noted that all EVC1-positive cells were dysplastic. Furthermore, EVC1 expression was clearly detected in a mouse ATL model that was established using xenotrans-

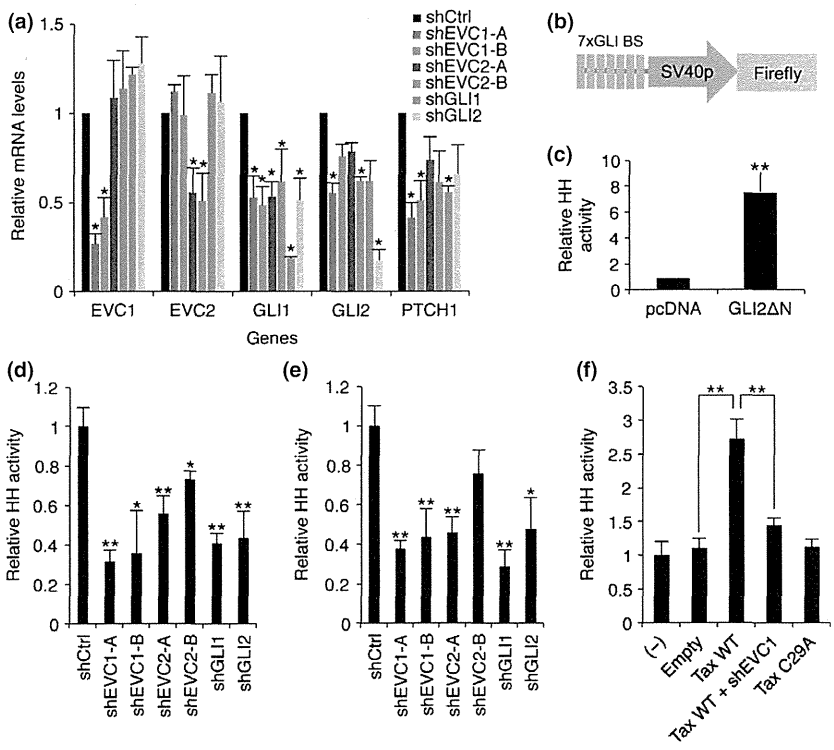

Fig. 5. EVC supports Hedgehog (HH) activity. (a) Relative RNA levels in shRNA-expressing TL-Om1 cells ($n = 3$, mean ± SD). $^{*}P < 0.05$. (b) Luciferase reporter plasmid containing 7 × sequential GLI-binding sites. (c) GLI2ΔN activa-ted HH activity ($n = 3$, mean ± SD). $^{**}P < 0.01$. (d–f) Hedgehog activity in various shRNA-expressing TL-Om1 (d), MT-2 (e) and Tax and shEVC1-expressing Jurkat (f) ($n = 3$–4, mean ± SD). $^{*}P < 0.05$. $^{**}P < 0.01$.

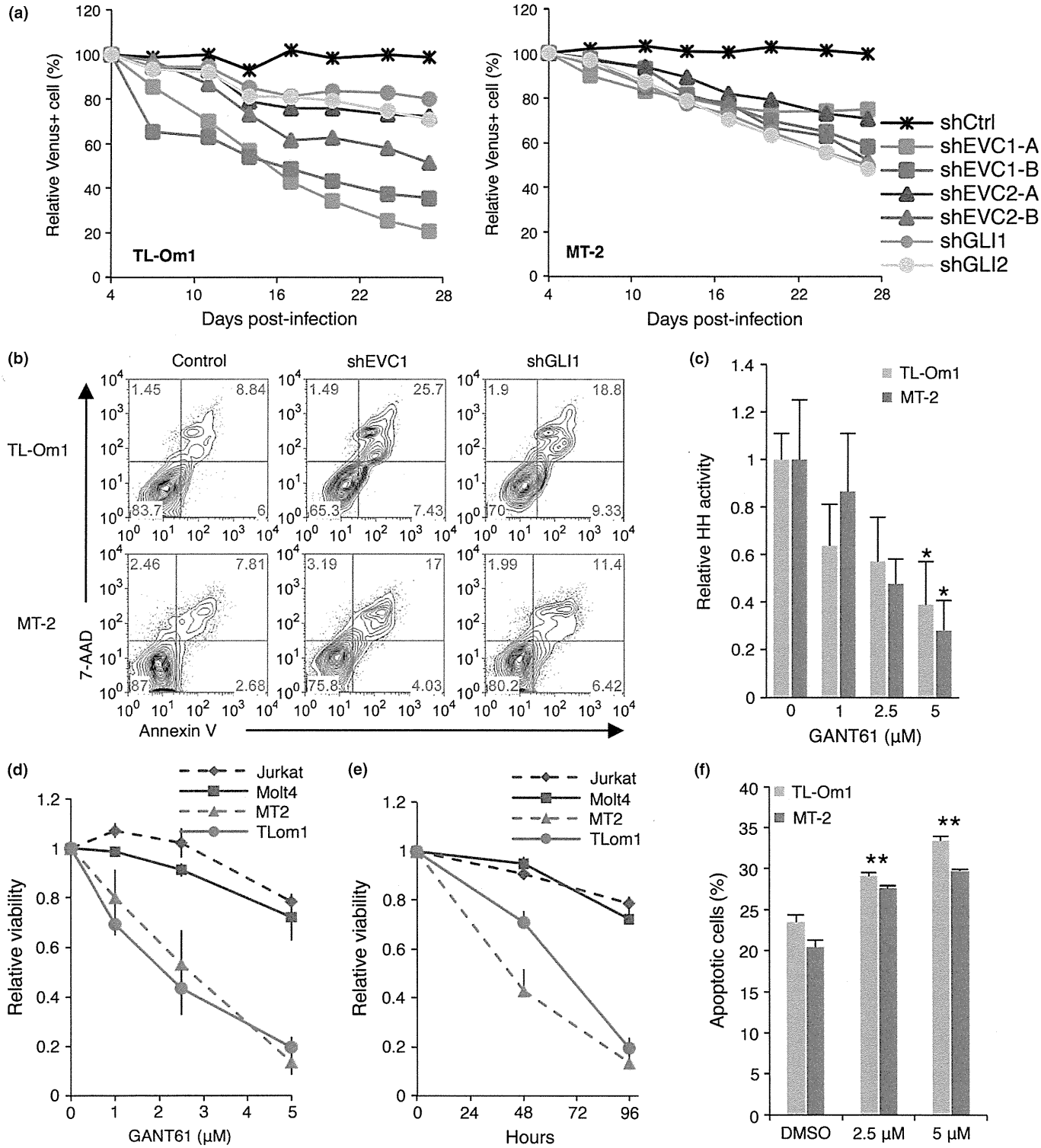

Fig. 6. Hedgehog (HH)-dependent ATL cell survival. (a) Time course of the abundance of Venus+ TL-Om1 (left) and MT-2 (right) infected with lentiviral vector expressing control shRNA (shCtrl), either of two shRNA targeting EVC1 and EVC2, or shRNA targeting GLI1 and GLI2, then cultured for 27 days together with uninfected cells. Data are representative of three independent experiments. Results are presented relative to those of cells at 4 days post-infection. (b) shRNA-mediated apoptosis induction. shRNA-expressing cells were cultured in 1% FBS for 72 h. The apoptotic pattern was defined by gating with Venus+ and Annexin V/7-AAD ($n = 3$, representative data). (c) GANT61 inhibited HH activity in ATL cells ($n = 3$, mean ± SD). $^*P < 0.05$. (d–e) GANT61 reduced ATL cell viability ($n = 3$, mean ± SD). The cells were treated with the indicated concentrations of GANT61 for 96 h (d) or with 5 μM of GANT61 for the indicated time periods (e). Cells were maintained in 1% FCS. (f) GANT61-dependent apoptosis analyzed using Annexin V/7-AAD staining ($n = 3$, mean ± SD). $^{**}P < 0.01$.

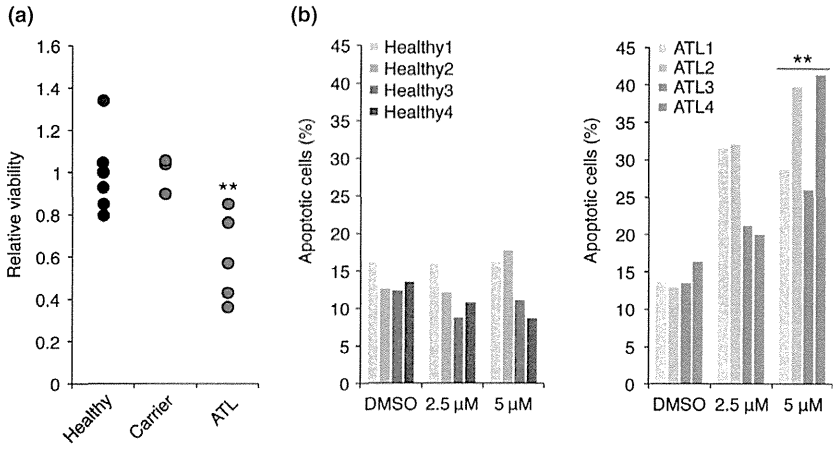

Fig. 7. GANT61 treatment reduced cell viabilities of primary ATL samples. (a) Effect of GANT61 in primary PBMC samples. The PBMC from healthy donors ($n = 7$), asymptomatic carriers ($n = 3$) and ATL patients ($n = 5$) were exposed in 5 μM of GANT61 for 72 h. Cells were maintained in media with 1% self-serum. $^{**}P < 0.01$. (b) GANT61-dependent apoptosis in ATL samples. The PBMC from healthy donors ($n = 4$) and ATL patients ($n = 4$) were treated with 5 μM of GANT61 for 72 h. Graphs show percentiles of apoptotic population in CD4+ cells $^{**}P < 0.01$.

plantation of primary tumor cells derived from an ATL patient. The lymphoma cells specifically expressed EVC1 (Fig. 4d,e). Taken together, EVC1 protein was definitely expressed in ATL cells.

EVC in HH activation. The EVC family has been implicated in HH signaling.[18,19] We performed the knockdown of EVC in TL-Om1 and MT-2 cells, which all highly expressed EVC (Fig. 1g). Specific knockdown was accomplished using lentivirus harboring specific and previously validated shRNA against EVC1, EVC2 or GLI transcription factors in the HH cascade. The qRT-PCR revealed the knockdown efficiency and also the HH activity as the RNA levels of *PTCH1* and *GLI1* were well-established HH activity markers.[29] The EVC depletion resulted in reduction of *PTCH1* and *GLI1* mRNA levels (Fig. 5a). Next we established a luciferase reporter containing 7 × sequential GLI-binding sites (Fig. 5b), which strongly responded against GLI2ΔN, a constitutive active form of GLI2[12] (Fig. 5c). As expected, the knockdown of EVC1 and EVC2 represented diminished HH activity in TL-Om1 and MT-2 cells (Fig. 5d,e). In addition, Tax activated the HH signal in Jurkat cells (Fig. 5f). Knockdown of EVC1 cancelled Tax-directed HH activation, suggesting that Tax affects HH signaling through, at least partially, EVC induction epigenetically.

EVC-dependent cell survival in ATL. Aberrant activation of HH provides cell survival ability in myeloma and lymphoma.[14,15] We found that different shRNA targeting EVC and GLI caused a progressive depletion of Venus+ cells (Fig. 6a). Knockdown of EVC1 or EVC2 attenuated ATL cell proliferation (Fig. S2). The growth defect was associated with a substantial decrease in the expression of targeted genes (Fig. 5). We then measured the apoptotic status by staining Annexin V/7-AAD. Specific analyses within the knocked down cells were achieved by gating with Venus fluorescence. At complete growth condition, slight but steady apoptosis was induced by EVC1 knockdown in MT-2 and TL-Om1 cells (data not shown). Furthermore, strong apoptosis was observed in EVC1-depleted cells at low FCS condition (Fig. 6b). This cell death appeared to be due to HH inactivation because GLI1-knocked down cells showed similar results.

Specific killing of ATL cell by GANT61. GANT61 is a cell-permeable hexahydropyrimidine compound, which has been shown to be a well-established inhibitor of GLI-mediated gene transactivation.[29] GANT61 treatment successfully reduced GLI binding to the target sequence (Fig. 6c). In that condition, MT-2 and TL-Om1 cells showed remarkable reduction of cell viability by GANT61 treatment in dose- and time-dependent manners (Fig. 6d,e), which may be caused by apoptosis (Fig. 6f).

Finally, we evaluated the pharmacological activity of GANT61 on primary ATL samples. Although GANT61 did not show a clear effect on PBMC derived from healthy donors and HTLV-1 carriers, its treatment specifically reduced the viability of ATL samples significantly (Fig. 7a). Flow cytometry demonstrated that GANT61 specifically killed CD4+ leukemic cells from ATL patients via apoptosis induction (Fig. 7b).

Discussion

A large number of efforts have collectively concluded that aberrant gene expression patterns contribute to the malignant characteristics in ATL and other neoplastic cells. In the present study, based on the careful analyses of patient samples, we have demonstrated that *EVC* is drastically overexpressed in mRNA and its protein can be specifically detected in ATL cells in contrast to normal CD4+ T-cells. To the best of our knowledge, this is the first report regarding EVC expression and function in lymphocytes. The results of the microarray indicate that *EVC* expression appears to be induced in accordance with disease progression. EVC1 protein expression is observed in dysplastic ATL cells derived from patients and a xenotransplantation model. Because the EVC family may be membrane-associated proteins (Fig. 4),[30] the present study provides us with the possibility that EVC expressions might be useful cell markers of HTLV-1-infected T-cells for future clinical purposes.

The EVC family has been identified initially as the responsible genes for one morphogenic disorder, Ellis van Creveld syndrome; it is also believed to play a role in the determination of body-axis or morphogenesis by usually bearing one step of the HH signaling pathway.[12,17–19] Knockout studies have demonstrated that EVC1 and EVC2 cooperatively act as positive modulators of the HH pathway in mouse fibroblasts and chondrocytes. However, abnormal EVC upregulation has not been reported in any cancers; whether the HH pathway is sensitive to cellular dynamism of EVC has not been elucidated as yet. Herein, we demonstrated that overexpression of EVC can be linked to HH activity in T cells for the first time. In addition, several experimental results, including the knockdown assay and GANT61 treatment, suggest totally that the HH pathway was activated in ATL, which in turn contributed to ATL cell survival. Further study will be required for mechanistic insights on how EVC activates HH in T cells.

Further investigation uncovered that transcription from the *EVC* locus was coordinated by epigenetic alteration. In particular, the lymphoma-associated H3Ac and H3K4me3 accumulations appeared to dominate EVC upregulation. Direct evidence from patient samples supported the epigenetic reprogramming, including previously unappreciated H3K4me3 rearrangements, conferring robust EVC expression. Interestingly, repressive histone mark H3K27me3 was mutually reduced at the *EVC* locus in the ATL samples, suggesting that cooperative regulation in this bivalent domain may define the EVC expression and possibly HH activity.

HTLV-1 Tax was involved in the regulation of EVC via epigenetic regulation. Nuclear localization-deficient Tax mutant was unable to induce EVC expression, implying that Tax may participate directly in determination of chromatin architecture. Indeed, lentiviral expression of Tax partially increased active histone modifications, which in turn activated HH signaling. Previously, we and others have reported that Tax physically binds with histone modifying factors, including HDAC,[31] SUV39H1[32] and SMYD3.[20] Interplay between Tax and epigenetic rearrangement may be closely involved in the progression of HTLV-1-infected cells to leukemic cells. Meanwhile, other ATL-specific epigenetic events including significant modifications on histone acetylation, H3K4me3 and H3K27me3 clearly dominate stable EVC expression. The alteration of the epigenetic landscape by Tax and other molecular mechanisms such as expression changes of epigenetic modifiers will be elucidated by comprehensive analysis such as a genome-wide ChIP analysis.

In the context of molecular targeting, a new possibility for the HH inhibitor was suggested. Recently, aberrant HH activation and its contribution to cell survival and the cell cycle have been reported in various cancer cells.[11,12] In agreement with other tumors where HH is active, we found that ATL was sensitive against GANT61. This compound can inhibit HH signaling by preventing DNA binding of the GLI family and has few impacts on the viability of healthy CD4+ T cells. We note that we could not confirm the EVC-directed upregulation of common HH target genes such as *Cyclin D1* and *Bcl-2* in ATL models (data not shown). Given that the HH pathway regulates transcription of many genes important for cell fate and many inhibitors against HH cascade have been developed,[16] our findings suggest that pharmacological drugs that can inhibit the HH pathway may be feasible for ATL treatment. Identification of ATL-specific HH target genes will help understanding of the HH roles in survival capability.

In summary, we have identified EVC overexpression as a specific character of ATL and HTLV-1-infected T cells. We have demonstrated the molecular mechanism that overexpressed EVC1 contributes to ATL cell survival. Considering aberrant gene expression associated with cancers, the emerging relationship between epigenetic regulation and the HH pathway provides us with conceptual advance in understanding the broad-acting oncogenic signaling.

Acknowledgments

The authors thank Dr M. Iwanaga and Ms T. Akashi for support and maintenance of JSPFAD and Mr Y. Sasaki for experimental support of the IHC study. The authors also thank Drs H. Miyoshi and A. Miyawaki for providing the Venus-encoding lentivirus vectors and Dr S. Okada for providing the NOJ mice. This work is supported by JSPS KAKENHI Grant Numbers 24790436 (M.Y.) and 23390250 (T.W.), MEXT KAKENHI Grant Number 221S0001 (T.W.), Grant-in-Aid from the Ministry of Health, Labour and Welfare H24-Third Term Cancer-004 (T.W.), and a grant from the Uehara Memorial Foundation (M.Y.).

Disclosure Statement

The authors have no conflict of interest.

References

1 Uchiyama T, Yodoi J, Sagawa K, Takatsuki K, Uchino H. Adult T-cell leukemia: clinical and hematologic features of 16 cases. *Blood* 1977; **50**: 481–92.
2 Poiesz BJ, Ruscetti FW, Gazdar AF, Bunn PA, Minna JD, Gallo RC. Detection and isolation of type C retrovirus particles from fresh and cultured lymphocytes of a patient with cutaneous T-cell lymphoma. *Proc Natl Acad Sci USA* 1980; **77**: 7415–9.
3 Yoshida M, Miyoshi I, Hinuma Y. Isolation and characterization of retrovirus from cell lines of human adult T cell leukemia and its implication in the disease. *Proc Natl Acad Sci USA* 1982; **79**: 2031–5.
4 Tsukasaki K, Utsunomiya A, Fukuda H *et al.* VCAP-AMP-VECP compared with biweekly CHOP for adult T-cell leukemia–lymphoma: Japan Clinical Oncology Group Study JCOG9801. *J Clin Oncol* 2007; **25**: 5458–64.
5 Yamagishi M, Nakano K, Miyake A *et al.* Polycomb-mediated loss of miR-31 activates NIK-dependent NF-κB pathway in adult T cell leukemia and other cancers. *Cancer Cell* 2012; **21**: 121–35.
6 Yamagishi M, Watanabe T. Molecular hallmarks of adult T cell leukemia. *Front Microbiol* 2012; **3**: 334.
7 Grassmann R, Aboud M, Jeang KT. Molecular mechanisms of cellular transformation by HTLV-1 Tax. *Oncogene* 2005; **24**: 5976–85.
8 Hall WW, Fujii M. Deregulation of cell-signaling pathways in HTLV-1 infection. *Oncogene* 2005; **24**: 5965–75.
9 Mori N, Fujii M, Ikeda S *et al.* Constitutive activation of NF-kappaB in primary adult T-cell leukemia cells. *Blood* 1999; **93**: 2360–8.
10 Watanabe M, Ohsugi T, Shoda M *et al.* Dual targeting of transformed and untransformed HTLV-1-infected T cells by DHMEQ, a potent and selective inhibitor of NF-kappaB, as a strategy for chemoprevention and therapy of adult T-cell leukemia. *Blood* 2005; **106**: 2462–71.
11 Low JA, de Sauvage FJ. Clinical experience with Hedgehog pathway inhibitors. *J Clin Oncol* 2010; **28**: 5321–6.
12 Briscoe J, Thérond PP. The mechanisms of Hedgehog signalling and its roles in development and disease. *Nat Rev Mol Cell Biol* 2013; **14**: 416–29.
13 Johnson RL, Rothman AL, Xie J *et al.* Human homolog of patched, a candidate gene for the basal cell nevus syndrome. *Science* 1996; **272**: 1668–71.
14 Dierks C, Grbic J, Zirlik K *et al.* Essential role of stromally induced hedgehog signaling in B-cell malignancies. *Nat Med* 2007; **13**: 944–51.
15 Singh RR, Kim JE, Davuluri Y *et al.* Hedgehog signaling pathway is activated in diffuse large B-cell lymphoma and contributes to tumor cell survival and proliferation. *Leukemia* 2010; **24**: 1025–36.
16 McMillan R, Matsui W. Molecular pathways: the hedgehog signaling pathway in cancer. *Clin Cancer Res* 2012; **18**: 4883–8.
17 Tompson SWJ, Ruiz-Perez VL, Blair HJ *et al.* Sequencing EVC and EVC2 identifies mutations in two-thirds of Ellis-van Creveld syndrome patients. *Hum Genet* 2007; **120**: 663–70.
18 Ruiz-Perez VL, Blair HJ, Rodriguez-Andres ME *et al.* Evc is a positive mediator of Ihh-regulated bone growth that localises at the base of chondrocyte cilia. *Development* 2007; **134**: 2903–12.
19 Dorn KV, Hughes CE, Rohatgi R. A Smoothened-Evc2 complex transduces the Hedgehog signal at primary cilia. *Dev Cell* 2012; **23**: 823–35.
20 Yamamoto K, Ishida T, Nakano K *et al.* SMYD3 interacts with HTLV-1 Tax and regulates subcellular localization of Tax. *Cancer Sci* 2011; **102**: 260–6.
21 Sasaki H, Hui C, Nakafuku M, Kondoh H. A binding site for Gli proteins is essential for HNF-3beta floor plate enhancer activity in transgenics and can respond to Shh *in vitro*. *Development* 1997; **124**: 1313–22.
22 Yamagishi M, Ishida T, Miyake A *et al.* Retroviral delivery of promoter-targeted shRNA induces long-term silencing of HIV-1 transcription. *Microbes Infect* 2009; **11**: 500–8.
23 Miyoshi H, Takahashi M, Gage FH, Verma IM. Stable and efficient gene transfer into the retina using an HIV-based lentiviral vector. *Proc Natl Acad Sci USA* 1997; **94**: 10319–23.

24 Miyoshi H, Blömer U, Takahashi M, Gage FH, Verma IM. Development of a self-inactivating lentivirus vector. *J Virol* 1998; **72**: 8150–7.
25 Kobayashi S, Nakano K, Watanabe E *et al.* CADM1 expression and stepwise downregulation of CD7 are closely associated with clonal expansion of HTLV-I-infected cells in adult T-cell leukemia/lymphoma. *Clin Cancer Res* 2014; **20**: 2851–61.
26 Sasaki D, Imaizumi Y, Hasegawa H *et al.* Overexpression of enhancer of zeste homolog 2 with trimethylation of lysine 27 on histone H3 in adult T-cell leukemia/lymphoma as a target for epigenetic therapy. *Haematologica* 2011; **96**: 712–9.
27 Smith MR, Greene WC. Identification of HTLV-I tax trans-activator mutants exhibiting novel transcriptional phenotypes. *Genes Dev* 1990; **4**: 1875–85.
28 Tsuji T, Sheehy N, Gautier VW, Hayakawa H, Sawa H, Hall WW. The nuclear import of the human T lymphotropic virus type I (HTLV-1) tax protein is carrier- and energy-independent. *J Biol Chem* 2007; **282**: 13875–83.
29 Lauth M, Bergström A, Shimokawa T, Toftgård R. Inhibition of GLI-mediated transcription and tumor cell growth by small-molecule antagonists. *Proc Natl Acad Sci USA* 2007; **104**: 8455–60.
30 Blair HJ, Tompson S, Liu YN *et al.* Evc2 is a positive modulator of Hedgehog signalling that interacts with Evc at the cilia membrane and is also found in the nucleus. *BMC Biol* 2011; **9**: 14.
31 Ego T, Ariumi Y, Shimotohno K. The interaction of HTLV-1 Tax with HDAC1 negatively regulates the viral gene expression. *Oncogene* 2002; **21**: 7241–6.
32 Kamoi K, Yamamoto K, Misawa A *et al.* SUV39H1 interacts with HTLV-1 Tax and abrogates Tax transactivation of HTLV-1 LTR. *Retrovirology* 2006; **3**: 5.

Supporting Information

Additional supporting information may be found in the online version of this article:

Fig. S1. HTLV-1 *HBZ* does not affect EVC expression.

Fig. S2. EVC knockdown reduces ATL cell proliferation.

Methods S1. Including: details of clinical samples; and primer sequences used in the present study.

Published OnlineFirst April 11, 2014; DOI: 10.1158/1078-0432.CCR-13-3169

Human Cancer Biology

Clinical Cancer Research

CADM1 Expression and Stepwise Downregulation of CD7 Are Closely Associated with Clonal Expansion of HTLV-I–Infected Cells in Adult T-cell Leukemia/Lymphoma

Seiichiro Kobayashi[1], Kazumi Nakano[5], Eri Watanabe[2], Tomohiro Ishigaki[2], Nobuhiro Ohno[3], Koichiro Yuji[3], Naoki Oyaizu[4], Satomi Asanuma[5], Makoto Yamagishi[5], Tadanori Yamochi[5], Nobukazu Watanabe[2], Arinobu Tojo[1,3], Toshiki Watanabe[5], and Kaoru Uchimaru[3]

Abstract

Purpose: Cell adhesion molecule 1 (CADM1), initially identified as a tumor suppressor gene, has recently been reported to be ectopically expressed in primary adult T-cell leukemia–lymphoma (ATL) cells. We incorporated CADM1 into flow-cytometric analysis to reveal oncogenic mechanisms in human T-cell lymphotrophic virus type I (HTLV-I) infection by purifying cells from the intermediate stages of ATL development.

Experimental Design: We isolated CADM1- and CD7-expressing peripheral blood mononuclear cells of asymptomatic carriers and ATLs using multicolor flow cytometry. Fluorescence-activated cell sorted (FACS) subpopulations were subjected to clonal expansion and gene expression analysis.

Results: HTLV-I–infected cells were efficiently enriched in $CADM1^{+}$ subpopulations (D, $CADM1^{pos}CD7^{dim}$ and N, $CADM1^{pos}CD7^{neg}$). Clonally expanding cells were detected exclusively in these subpopulations in asymptomatic carriers with high proviral load, suggesting that the appearance of D and N could be a surrogate marker of progression from asymptomatic carrier to early ATL. Further disease progression was accompanied by an increase in N with a reciprocal decrease in D, indicating clonal evolution from D to N. The gene expression profiles of D and N in asymptomatic carriers showed similarities to those of indolent ATLs, suggesting that these subpopulations represent premalignant cells. This is further supported by the molecular hallmarks of ATL, that is, drastic downregulation of miR-31 and upregulation of abnormal *Helios* transcripts.

Conclusion: The CADM1 versus CD7 plot accurately reflects disease progression in HTLV-I infection, and $CADM1^{+}$ cells with downregulated CD7 in asymptomatic carriers have common properties with those in indolent ATLs. *Clin Cancer Res; 20(11); 2851–61. ©2014 AACR.*

Introduction

Human T-cell lymphotrophic virus type I (HTLV-I) is a human retrovirus that causes HTLV-I–associated diseases, such as adult T-cell leukemia–lymphoma (ATL), HTLV-I–associated myelopathy/tropical spastic paraparesis, and HTLV-I uveitis (1–3). In Japan, the estimated lifetime risk of developing ATL in HTLV-I carriers is 6% to 7% for males and 2% to 3% for females (4–6). It takes several decades for HTLV-I–infected cells to reach the final stage of multistep oncogenesis, which is clinically recognized as aggressive ATL (acute-type and lymphoma-type; ref. 7). Molecular interaction of viral genes [e.g., Tax and the HTLV-I basic leucine zipper (HBZ) gene] with the cellular machinery causes various genetic and epigenetic alterations (7–11). However, difficulties in purifying HTLV-I–infected cells *in vivo* seem to have hindered understanding of the genetic events that are directly involved in the multistep oncogenesis of ATL.

Upregulation or aberrant expression of cell surface markers, such as CCR4 and CD25, is useful for diagnosis of ATL and has been utilized for molecular-targeted therapy (12, 13). However, the expression levels of these markers vary among patients, which often make it difficult to identify ATL cells specifically based on the immunophenotype. Previously, we focused on downregulated markers in acute-type ATL cells, such as CD3 and CD7, and successfully purified ATL cells using the CD3 versus CD7 plot of $CD4^{+}$ cells (14). Analysis of other clinical subtypes

Authors' affiliations: [1]Division of Molecular Therapy; [2]Laboratory of Diagnostic Medicine, Division of Stem Cell Therapy; [3]Department of Hematology/Oncology, Research Hospital; [4]Clinical Laboratory, Research Hospital, Institute of Medical Science; and [5]Graduate School of Frontier Sciences, The University of Tokyo, Tokyo, Japan

Note: Supplementary data for this article are available at Clinical Cancer Research Online (http://clincancerres.aacrjournals.org/).

Corresponding Author: Kaoru Uchimaru, Institute of Medical Science, The University of Tokyo, 4-6-1 Shirokanedai, Minato-ku, Tokyo 108-8639, Japan. Phone: 81-3-5449-5542; Fax: 81-3-5449-5429; E-mail: uchimaru@ims.u-tokyo.ac.jp

doi: 10.1158/1078-0432.CCR-13-3169

Published OnlineFirst April 11, 2014; DOI: 10.1158/1078-0432.CCR-13-3169

Translational Relevance

In this study, we showed that the cell adhesion molecule 1 (CAMD1) versus CD7 plot reflects the progression of disease in patients infected with human T-cell lymphotrophic virus type I (HTLV-I), in that the proportion of $CADM1^{+}$ subpopulations (D, $CADM1^{pos}$ $CD7^{dim}$ and N, $CADM1^{pos}CD7^{neg}$) increased with the progression from HTLV-I asymptomatic carrier (AC) to indolent adult T-cell leukemia–lymphoma (ATL) to aggressive ATL. We confirmed the purity of the clonal HTLV-I–infected cells in these subpopulations of various clinical subtypes, including asymptomatic carriers. The results from the flow-cytometric analysis will help physicians assess disease status. The analysis is also practical in screening for putative high-risk HTLV-I asymptomatic carriers, which show nearly identical flow-cytometric and gene expression profiles with those of smoldering-type ATL patients. Furthermore, cell sorting by flow cytometry enables purification of clonally expanding cells in various stages of oncogenesis in the course of progression to aggressive ATL. Detailed molecular analysis of these cells will provide valuable information about the molecular events involved in multistep oncogenesis of ATL.

(indolent ATLs and HTLV-I asymptomatic carriers; AC) revealed that HTLV-I–infected and clonally expanded cells were purified similarly and that the subpopulations with downregulated CD7 grew concomitantly with the progression of HTLV-I infection (15). Although this type of flow-cytometric analysis was shown to be a useful tool, a substantial subpopulation of T cells shows downregulated expression of CD7 under physiologic (16, 17) and certain pathologic conditions, including autoimmune disorders, viral infection, and hematopoietic stem cell transplantation (18–23).

Recently, Sasaki and colleagues reported ectopic overexpression of the cell adhesion molecule 1/tumor suppressor in lung cancer 1 (CADM1/TSLC1) gene in primary acute-type ATL cells based on expression profile analysis (24, 25). CADM1 (/TSLC1) is a cell-adhesion molecule that was originally identified as a tumor suppressor in lung cancers (25, 26). In addition, numbers of $CD4^{+}$ $CADM1^{+}$ cells have been found to be significantly correlated with the proviral load (PVL) in both ATLs and HTLV-I asymptomatic carriers (25, 27). Thus, CADM1 is a good candidate marker of HTLV-I–infected cells. In the present study, we incorporated CADM1 into our flow-cytometric analysis. In the CADM1 versus CD7 plot of $CD4^{+}$ cells, HTLV-I–infected and clonally expanded cells were efficiently enriched in the $CADM1^{+}$ subpopulations regardless of disease status. In these cells, stepwise CD7 downregulation (from dimly positive to negative) occurred with disease progression. The proportion of the three subpopulations observed in this plot [P, $CADM1^{negative(neg)}CD7^{positive(pos)}$; D, $CADM1^{pos}CD7^{dim}$; and N, $CADM1^{pos}$ $CD7^{neg}$] accurately reflected the disease status in HTLV-I infection. The analysis of comprehensive gene expression in each subpopulation revealed that the expression profile of $CADM1^{+}$ subpopulations in indolent ATLs showed similarities with that in asymptomatic carriers with high PVL; yet, it was distinct from that in aggressive ATLs. These D and N subpopulations were indicative of HTLV-I–infected cells in the intermediate stage of ATL development.

Materials and Methods

Cell lines and patient samples

TL-Om1, an HTLV-I–infected cell line (28), was provided by Dr. Sugamura (Tohoku University, Sendai, Japan). The MT-2 cell line was a gift from Dr. Miyoshi (Kochi University, Kochi, Japan) and ST-1 was from Dr. Nagai (Nagasaki University, Nagasaki, Japan). Peripheral blood samples were collected from in-patients and out-patients at our hospital, as described in our previous reports (14, 15). As shown in Supplementary Table S1, 26 cases were analyzed (10 cases of asymptomatic carrier; 5 cases of smoldering-type; 6 cases of chronic-type; and 5 cases of acute-type). All patients with ATL were categorized into clinical subtypes according to Shimoyama's criteria (12, 29). Patients with various complications, such as autoimmune disorders and systemic infections, were excluded. Lymphoma-type patients were also excluded because ATL cells are not considered to exist in the peripheral blood of this clinical subtype. Samples collected from six healthy volunteers (mean age 48.8 years; range 34–66 years) were used as normal controls. The present study was approved by the Institutional Review Board of our institute (the University of Tokyo, Tokyo, Japan). Written informed consent was obtained from all patients and healthy volunteers.

Flow cytometry and cell sorting

Peripheral blood mononuclear cells (PBMC) were isolated from whole blood by density gradient centrifugation, as described previously (14). An unlabeled CADM1 antibody (clone 3E1) and an isotype control chicken immunoglobulin Y (IgY) antibody were purchased from MBL. These were biotinylated (primary amine biotinylation) using biotin N-hydroxysuccinimide ester (Sigma-Aldrich). Pacific Orange-conjugated anti-CD14 antibody was purchased from Caltag-Invitrogen. All other antibodies were obtained from BioLegend. Cells were stained using a combination of biotin-CADM1, allophycocyanin (APC)-CD7, APC-Cy7-CD3, Pacific Blue-CD4, and Pacific Orange-CD14. After washing, phycoerythrin-conjugated streptavidin was applied. Propidium iodide (Sigma-Aldrich) was added to the samples to stain dead cells immediately before flow cytometry. A FACSAria instrument (BD Immunocytometry Systems) was used for all multicolor flow cytometry and fluorescence-activated cell sorting (FACS). Data were analyzed using FlowJo software (TreeStar). The gating

Published OnlineFirst April 11, 2014; DOI: 10.1158/1078-0432.CCR-13-3169

procedure for a representative case is shown in Supplementary Fig. S1.

Quantification of HTLV-I proviral load by real-time quantitative PCR

PVL in FACS-sorted PBMCs was quantified by real-time quantitative PCR (TaqMan method) using the ABI Prism 7000 sequence detection system (Applied Biosystems), as described previously (14, 30).

Evaluation of HTLV-I *HBZ* gene amplification by semiquantitative PCR

HTLV-I *HBZ* gene amplification was performed as described previously (25). Briefly, the 25-μL PCR mixture consisted of 20 pmol of each primer, 2.0 μL of mixed deoxynucleotide triphosphates (2.5 mmol/L each), 2.5 μL of 10× PCR buffer, 1.5 μL of $MgCl_2$ (25 mmol/L), 0.1 μL of AmpliTaq Gold DNA Polymerase (Applied Biosystems), and 20 ng of DNA extracted from cell lines and clinical samples. The PCR consisted of initial denaturation at 94°C for 9 minutes, 30 cycles of 94°C for 30 seconds, 57°C for 30 seconds, and 72°C for 45 seconds, followed by 72°C for 5 minutes. The β-actin gene (*ACTB*) was used as an internal reference control. The primer sequences used were as follows: HBZ forward, 5′-CGCTGCCGATCACGATG-3′; HBZ reverse, 5′-GGAGGAATTGGTGGACG-3′; ACTB forward, 5′-CGTGCTCAGGGCTTCTT-3′; and ACTB reverse, 5′-TGAAGGTCTCAAACATGATCTG-3′. Amplification with these pairs of oligonucleotides yielded 177-bp HBZ and 731-bp β-actin fragments.

FISH for quantification of HTLV-I–infected cells

FISH analysis was performed to detect HTLV-I proviral DNA in mononuclear cells that had been FACS-sorted on the basis of the CADM1 versus CD7 plot. These samples were sent to a commercial laboratory (Chromosome Science Labo Inc.), where FISH analysis was performed. Briefly, pUC/HTLV-I plasmid containing the whole-HTLV-I genome was labeled with digoxigenin by the nick translation method, and was then used as a FISH probe. Pretreatment, hybridization, and washing were performed according to standard laboratory protocols. To remove fluorochrome-labeled antibodies attached to the cell surface, pretreatment consisted of treatment with 0.005% pepsin and 0.1 N HCl. The FISH probe was detected with Cy3-labeled anti-digoxigenin antibody. Cells were counterstained with 4′, 6 diamidino-2-phenylindole. The results were visualized using a DMRA2 conventional fluorescence microscope (Leica) and photographed using a Leica CW4000 cytogenetics workstation. Hybridization signals were evaluated in approximately 100 nuclei.

Inverse long PCR to assess the clonality of HTLV-I–infected cells

For clonality analysis, inverse long PCR was performed as described previously (14). First, 1 μg genomic DNA extracted from the FACS-sorted cells was digested with *Pst*I or *Eco*RI at 37°C overnight. RNase A (Qiagen) was added to remove residual RNA completely. DNA fragments were purified using a QIAEX2 Gel Extraction Kit (Qiagen). The purified DNA was self-ligated with T4 DNA ligase (Takara Bio) at 16°C overnight. After ligation of the *Eco*RI-digested samples, the ligated DNA was further digested with *Mlu*I, which cuts the pX region of the HTLV-I genome and prevents amplification of the viral genome. Inverse long PCR was performed using Tks Gflex DNA Polymerase (Takara Bio). For the *Pst*I-treated group, the forward primer was 5′-CAGCCCATTCTATAGCACTCTCCAGGAGAG-3′ and the reverse primer was 5′-CAGTCTCCAAACACGTAGACTGGGTATCCG-3′. For the *Eco*RI-treated template, the forward primer was 5′-TGCCTGACCCTGCTTGCTCAACTCTACGTCTTTG-3′ and the reverse primer was 5′-AGTCTGGGCCCTGACCTTTTCAGACTTCTGTTTC-3′. Processed genomic DNA (50 ng) was used as a template. The reaction mixture was subjected to 35 cycles of denaturation (94°C, 30 seconds) and annealing plus extension (68°C, 8 minutes). Following PCR, the products were subjected to electrophoresis on 0.8% agarose gels. Fourteen patient samples were analyzed. For samples from which a sufficient amount of DNA was extracted, PCR was generally performed in duplicate.

Gene expression microarray analysis of each subpopulation in the CADM1 versus CD7 plot

Total RNA was extracted from each subpopulation in the CADM1 versus CD7 plot using TRIzol (Invitrogen) according to the manufacturer's protocol. Details of the clinical samples used for microarray analyses are shown in Supplementary Table S1. Treatment with DNase I (Takara Bio) was conducted to eliminate genomic DNA contamination. The quality of the extracted RNA was assessed using a BioAnalyzer 2000 system (Agilent Technologies). The RNA was then Cy3-labeled using a Low Input Quick Amp Labeling Kit (Agilent Technologies). Labeled cRNA samples were hybridized to 44K Whole Human Genome Oligonucleotide Microarrays (Agilent Technologies) at 65°C for 17 hours. After hybridization, the microarrays were washed and scanned with a Scanner C (Agilent Technologies). Signal intensities were evaluated by Feature Extraction 10.7 software and then analyzed using Gene Spring 12.0 software (Agilent Technologies). Unsupervised two-dimensional hierarchical clustering analysis (Pearson correlation) was performed on 10,278 genes selected by one-way ANOVA ($P < 0.05$). The dataset for these DNA microarrays has been deposited in Gene Expression Omnibus (accession number GSE55851).

Expression analysis of miR-31 and *Helios* transcript variants of each subpopulation in the CADM1 versus CD7 plot

The expression levels of the microRNA miR-31 were quantified using a TaqMan-based MicroRNA Assay (Applied Biosystems), as described previously (31), and normalized to RNU48 expression level. Helios mRNA transcript variants were examined using reverse transcription

Published OnlineFirst April 11, 2014; DOI: 10.1158/1078-0432.CCR-13-3169

PCR (RT-PCR) with Platinum Taq DNA Polymerase High Fidelity (Invitrogen), as described previously (32). To detect and distinguish alternative splicing variants, PCR analyses were performed with sense and antisense primer sets specific for the first and final exons of the Helios gene. The PCR products were then sequenced to determine the exact type of transcript variant. A mixture of Hel-1, Hel-2, Hel-5, and Hel-6 cDNA fragments was used as a "Helios standard" in the electrophoresis of RT-PCR samples.

Results

CADM1 expression based on the CD3 versus CD7 plot in CD4$^+$ cells in primary HTLV-I–infected blood samples

The clinical profiles of the 32 cases analyzed are shown in Supplementary Table S1. We first examined CADM1 expression in each subpopulation (H, I, and L) of the CD3 versus CD7 plot. Representative data (for a case of smoldering ATL) are shown in Fig. 1A. The results demonstrate that

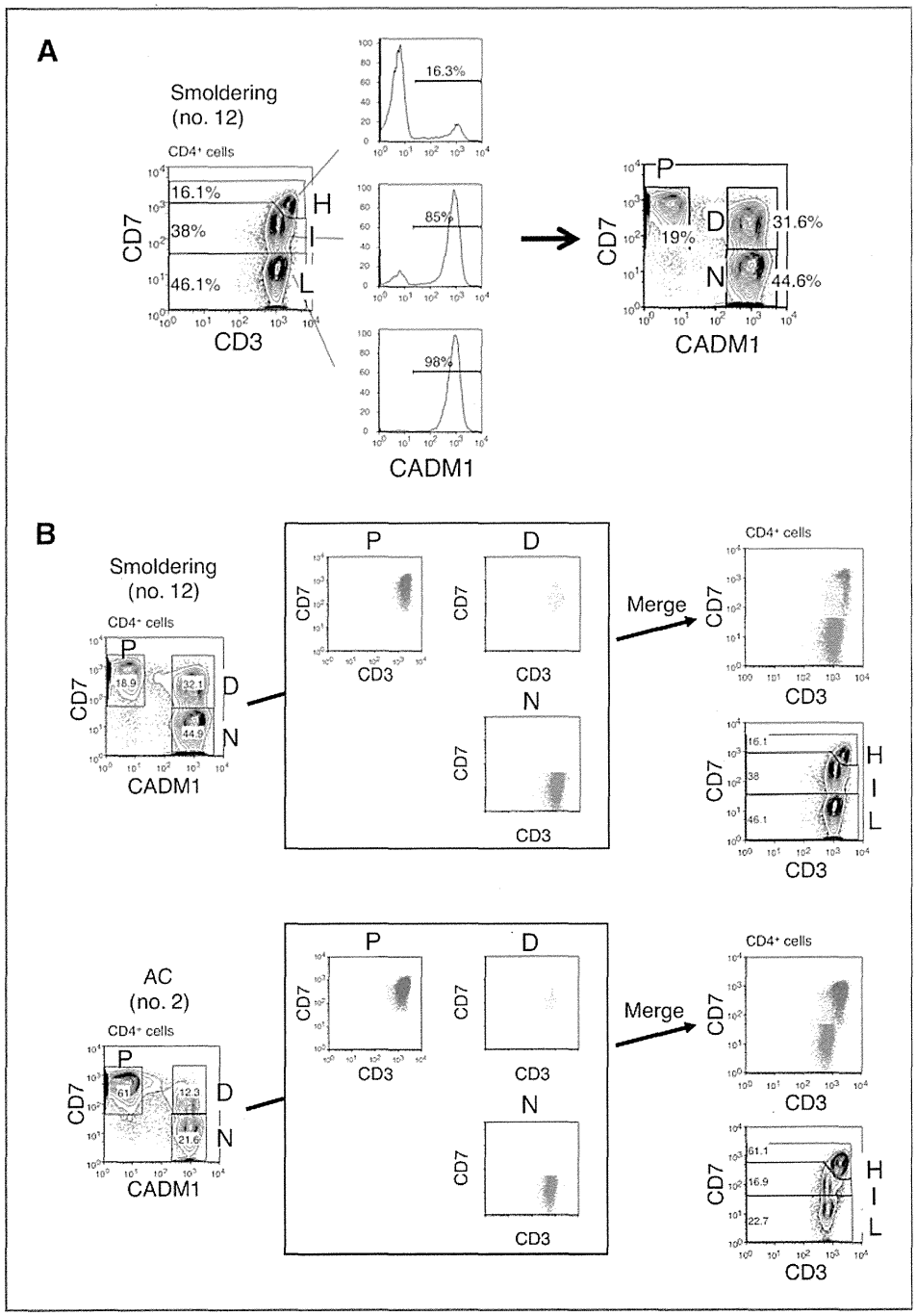

Figure 1. CADM1 versus CD7 plot for CD4$^+$ cells from HTLV-I–infected blood samples analyzed by flow cytometry. A, representative flow-cytometric analysis of a patient with smoldering-type ATL. Three subpopulations (H, I, and L) were observed in the CD3 versus CD7 plot for CD4$^+$ cells (left). Expression of CADM1 in each subpopulation is shown (middle). The right-hand panel shows how the CADM1 versus CD7 plot for CD4$^+$ cells was constructed. B, the P, D, and N subpopulations in the CADM1 versus CD7 plot correspond to the H, I, and L subpopulations in the CD3 versus CD7 plot. Blue, yellow, and red dots, respectively, indicate the P, D, and N subpopulations in the CADM1 versus CD7 plot, and are redrawn in the CD3 versus CD7 plot. Two representative cases are shown. In the upper case, the P and D subpopulations in the CADM1 versus CD7 plot are partly intermingled in the CD3 versus CD7 plot. Unlike the CD3 versus CD7 plot, the CADM1 versus CD7 plot clearly distinguishes three subpopulations.

Published OnlineFirst April 11, 2014; DOI: 10.1158/1078-0432.CCR-13-3169

CADM1 was expressed almost exclusively in the I and L subpopulations. Drawing a CADM1 versus CD7 plot for $CD4^+$ cells revealed three distinct subpopulations (P, $CADM1^{neg}CD7^{pos}$; D, $CADM1^{pos}CD7^{dim}$; and N, $CADM1^{pos}$ $CD7^{neg}$). As shown in Fig. 1B, the P, D, and N subpopulations corresponded to the H, I, and L subpopulations in the CD3 versus CD7 plot. In the previous CD3 versus CD7 plot, the lower case (AC no. 2) showed three distinct subpopulations. However, in the upper case (smoldering no. 12), the H and I subpopulations substantially intermingled with each other and were not clearly separated. In contrast, the CADM1 versus CD7 plot clearly revealed three distinct subpopulations in both cases.

HTLV-I–infected cells are highly enriched in $CADM1^+$ subpopulations

On the basis of previous reports (25, 27), we expected HTLV-I–infected cells to be enriched in the $CADM1^+$ subpopulations in our analysis. Figure 2A shows the PVL measurements of the three subpopulations in the CADM1 versus CD7 plot for three representative cases. HTLV-I–infected cells were highly enriched in the $CADM1^+$ subpopulations (D and N). The PVL data indicate that most of the cells in the D and N subpopulations were HTLV-I infected. Figure 2B shows the results of semiquantitative PCR of the *HBZ* gene in representative cases. In the D and N subpopulations, the *HBZ* gene was amplified to the same degree as in the HTLV-I–positive cell line. To confirm these results, FISH was performed in one asymptomatic carrier. As shown in Supplementary Fig. S2, HTLV-I–infected cells were highly enriched in the D and N subpopulations, which supports the results of the PVL analysis and semiquantitative PCR of the *HBZ* gene. In the FISH analysis, percentages of HTLV-I–infected cells in D and N did not reach 100%. This may have been due to a technical issue. Because the cells subjected to FISH analysis were sorted by FACS, several fluorochrome-conjugated antibodies may have remained on their surfaces, even after treatment with protease.

The CADM1 versus CD7 plot accurately reflects disease progression in HTLV-I infection

Compared with the CD3 versus CD7 plot, the CADM1 versus CD7 plot was revealed to be clear in its distinction of the three subpopulations and efficient in enrichment of HTLV-I–infected cells. On the basis of these findings, we analyzed clinical samples of asymptomatic carriers and three clinical subtypes of ATL: the smoldering, chronic, and acute subtypes. Data for representative cases, presented in Fig. 3A, suggest that the continual changes in the proportions of the three subpopulations are associated with disease progression. In the CADM1 versus CD7 plot, normal control samples showed a P-dominant pattern. With progression of the disease from the asymptomatic carrier state with a low PVL to that with a high PVL, and to indolent-type ATL, the D and N subpopulations increased gradually. As the disease further progressed to acute-type ATL, the N subpopulation showed remarkable expansion. Data for all analyzed samples are presented in Fig. 3B. The results suggest that the CADM1 versus CD7 plot of peripheral blood samples represents progression of the disease in HTLV-I carriers. Data for the normal control cases analyzed are shown in Supplementary Fig. S3. In all normal controls, the percentages of the D and N subpopulations were low. Supplementary Fig. S4 shows temporal data for a patient with chronic-type ATL who progressed from stable disease to a relatively progressive state and the concomitant change in the flow cytometry profile.

Clonality analysis of the three subpopulations in the CADM1 versus CD7 plot

To characterize the three subpopulations further, the clonal composition of each subpopulation was analyzed by inverse long PCR, which amplifies part of the provirus

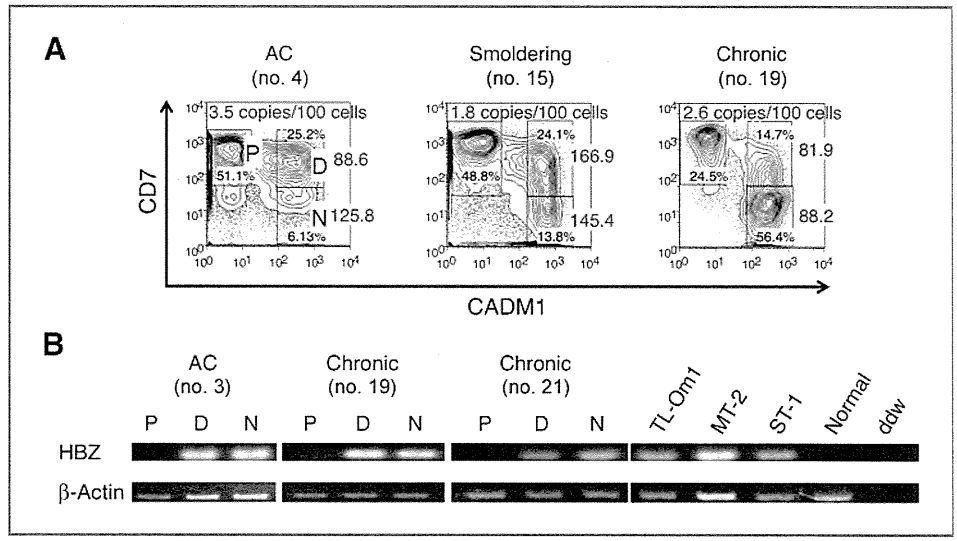

Figure 2. HTLV-I–infected cells are highly enriched in the $CADM1^+$ subpopulations. A, analysis of PVL in the three subpopulations. Three representative cases are shown. PVL data (copies/100 cells) are shown in red. Percentages of each subpopulation are shown in black. B, semiquantitative PCR of the *HBZ* gene in the three subpopulations in three representative cases. Normal, DNA from PBMCs from a normal control; ddw, deionized distilled water.

Published OnlineFirst April 11, 2014; DOI: 10.1158/1078-0432.CCR-13-3169

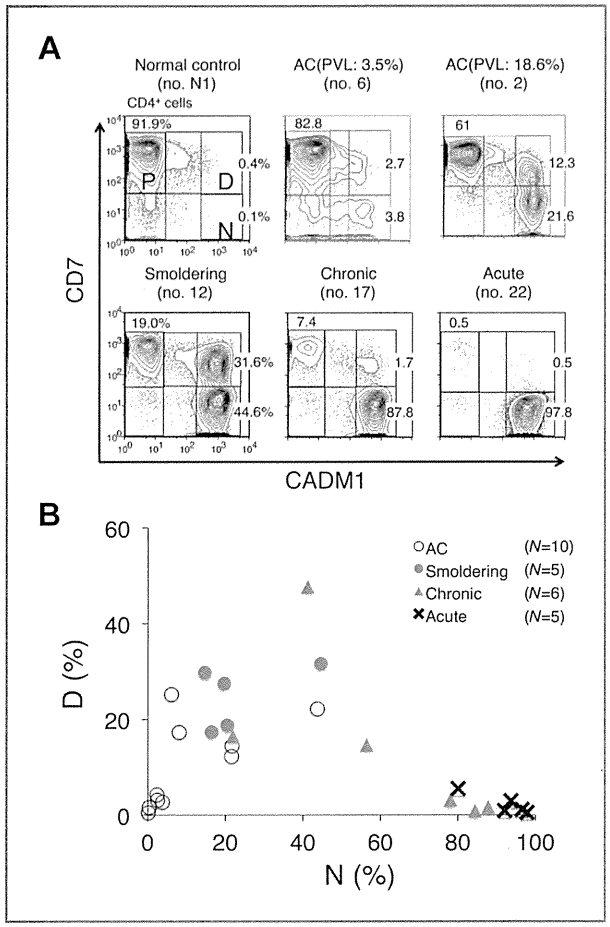

Figure 3. Proportion of each subpopulation in the CADM1 versus CD7 plots for asymptomatic HTLV-I carriers (asymptomatic carriers) and ATLs of various clinical subtypes. A, data of representative cases are shown. B, a two-dimensional plot of all analyzed samples showing the percentages of the D and N subpopulations.

long terminal repeat and the flanking genomic sequence of the integration sites. Cells in each subpopulation were sorted by FACS, and subjected to inverse long PCR analysis. Representative results for smoldering-, chronic-, and acute-type ATL samples are presented in Fig. 4A. Major clones, indicated by intense bands, were detected in the D and N subpopulations. The major clones in the D and N subpopulations in each case were considered to be the same based on the sizes of the amplified bands, suggesting that clonal evolution is accompanied by downregulation of CD7 expression. Fig. 4B shows representative results for three cases of asymptomatic carrier. In all cases, weak bands in the P subpopulation were visible, indicating that this population contains only minor clones. In these asymptomatic carriers, the proportion of abnormal lymphocytes and PVL increases from left to right. The consistent increase in the D and N subpopulations, together with growth of major clones as shown in the inverse PCR analysis, were considered to reflect these clinical data.

Gene expression profiling of the three subpopulations in the CADM1 versus CD7 plot

To determine the molecular basis for the biologic differences among the three subpopulations in the CADM1 versus CD7 plot, we next characterized the gene-expression profiles of the subpopulations of the following clinical subgroups: asymptomatic carriers ($n = 2$), smoldering-type ATLs ($n = 2$), chronic-type ATL ($n = 1$), acute-type ATLs ($n = 3$), and normal controls ($n = 3$). The two asymptomatic carriers (nos. 5 and 9) had high PVLs (11.6 and 26.2%, respectively) and relatively high proportions of D and N subpopulations (Supplementary Table S1). Unsupervised hierarchical clustering analysis of the results revealed three clusters (A, B1, and B2) or two major clusters A and B, where A is composed solely of the samples of the acute-type N subpopulation and B is subdivided into two clusters (B1 and B2; Fig. 5A). The B2 cluster is composed of the P subpopulation of all clinical subtypes and of normal controls, whereas the B1 cluster is composed of the D and N subpopulations of

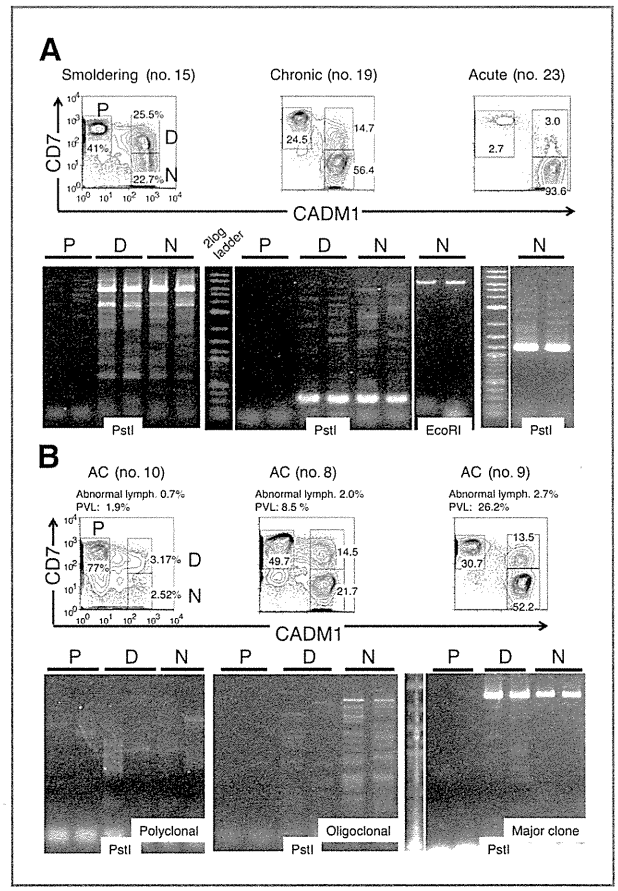

Figure 4. Clonality of subpopulations in the CADM1 versus CD7 plot analyzed by inverse long PCR. FACS-sorted cells (P, D, and N) were subjected to inverse long PCR. The black bar indicates duplicate data. Flow-cytometric profiles and clinical data are also presented. A, representative cases of smoldering-, chronic-, and acute-type ATL are shown. B, representative cases of asymptomatic carriers are shown.

Published OnlineFirst April 11, 2014; DOI: 10.1158/1078-0432.CCR-13-3169

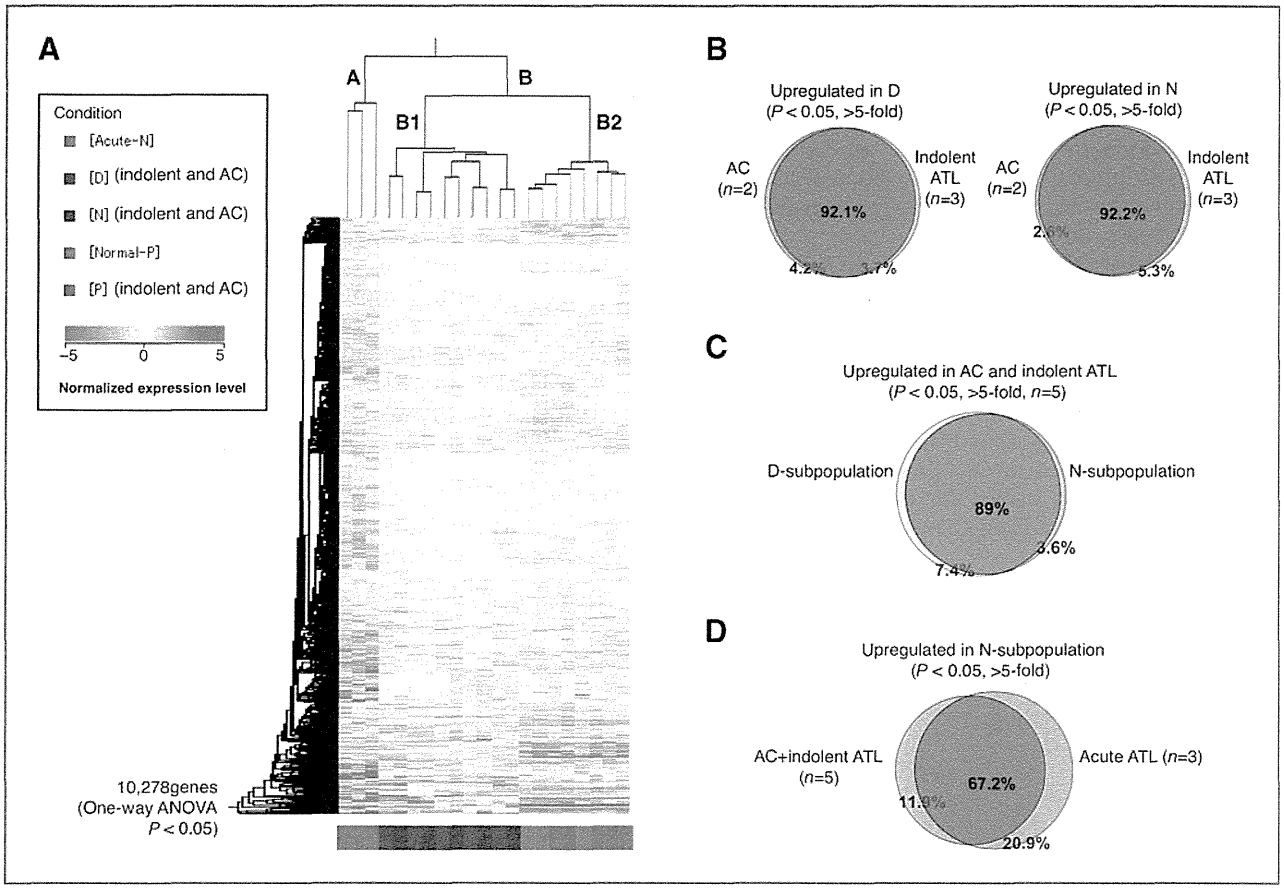

Figure 5. Comprehensive gene expression analysis of the three subpopulations in the CADM1 versus CD7 plot. A, we conducted an unsupervised hierarchical clustering analysis of 10,278 genes whose expression levels were significantly changed in the P subpopulation of normal controls ($n = 3$); P, D, and N subpopulations of asymptomatic carriers and indolent ATLs ($n = 5$); and N subpopulation of acute-ATLs ($n = 3$; one-way ANOVA, $P < 0.05$). The P and D subpopulations of acute ATLs and D and N subpopulations of normal controls could not be analyzed because of insufficient numbers of cells. Clustering resulted in three major clusters: (i) P subpopulations of normal controls (gray) and asymptomatic carriers/indolent ATLs (green); (ii) D and N subpopulations of asymptomatic carriers/indolent ATLs (blue and brown, respectively); and (iii) N subpopulations of acute ATLs (red). These results indicate that the P subpopulations of asymptomatic carriers/indolent ATLs have characteristics similar to those of normal uninfected cells, whereas the D and N subpopulations of asymptomatic carriers/indolent ATLs have genetic lesions in common. The N subpopulations of acute ATLs are grouped in an independent cluster, meaning that these malignant cell populations have a significantly different gene expression profile, even compared with the N subpopulations of indolent ATLs. B, similarity between asymptomatic carriers and indolent ATLs. The Venn diagrams show that 92.1% and 92.2% of genes upregulated in the D and N subpopulations, respectively, compared with "Normal-P" ($P < 0.05$), were common to asymptomatic carriers ($n = 2$) and indolent ATLs ($n = 3$). C, similarity between the D and N subpopulations. The Venn diagram shows that 89% of genes upregulated in the D and N subpopulation, compared with Normal-P ($P < 0.05$), overlapped. D, comparison of the N subgroups between acute-ATLs ($n = 3$) and asymptomatic carriers/indolent ATLs ($n = 5$). As shown in the Venn diagram, 67.2% of genes were upregulated ($P < 0.05$) in the N subpopulations of both acute ATLs and asymptomatic carrier/indolent ATLs. However, a significant number of genes (20.9%) were upregulated only in the N subpopulation of acute ATLs.

asymptomatic carriers and indolent ATLs (smoldering- and chronic-type).

Figure 5B shows a Venn diagram of the upregulated genes in the D subpopulation (left) or the N subpopulation (right) common to asymptomatic carriers ($n = 2$) and indolent ATLs ($n = 3$). These diagrams demonstrate that the changes in the gene expression profiles of the D and N subpopulations of asymptomatic carriers were similar to those of indolent ATLs. Furthermore, the gene expression profiles of the D and N subpopulations of asymptomatic carriers and indolent ATLs were similar (Fig. 5C). In contrast, the upregulated genes showed distinct differences between the N subpopulation of acute-type ATL and that of indolent ATLs and asymptomatic carriers, although approximately 70% were common to both (Fig. 5D).

Expression of a tumor suppressor microRNA and splicing abnormalities of Ikaros family genes in the three subpopulations

To determine whether the novel subpopulations identified had other properties in common with ATL cells, we examined miR-31 levels and *Helios* mRNA patterns in sorted subpopulations (31, 32). Expression of miR-31 decreased drastically in the D subpopulation derived from indolent ATLs and asymptomatic carriers, and was

Published OnlineFirst April 11, 2014; DOI: 10.1158/1078-0432.CCR-13-3169

even lower in the N subpopulation derived from asymptomatic carriers and indolent/acute ATLs (Fig. 6A). In addition, examination of *Helios* mRNA transcript variants revealed that expression levels of *Hel-2*, which lacks part of exon 3, were upregulated in the D and N subpopulations of asymptomatic carriers and indolent ATLs, and it was dominantly expressed in the N subpopulation of acute ATLs (Fig. 6B).

Supplementary Fig. S5 presents a summary of this study. The representative flow-cytometric profile shows how the CADM1 versus CD7 plot reflects disease progression in HTLV-I infection. The plot together with the gene expression profiles clearly distinguished the subpopulations of distinct oncogenic stages. The groups classified according to gene expression profile are shown as blue, yellow, and red and are superimposed on the CADM1 versus CD7 plot. Collectively, our data suggest that CADM1 expression and stepwise downregulation of CD7 were closely associated with clonal expansion of HTLV-I–infected cells in ATL progression.

Discussion

We showed that the CADM1 versus CD7 plot is capable of discriminating clonally expanding HTLV-I–infected cells in indolent ATLs and even in asymptomatic carriers, as well as in acute-type ATLs. Our analysis demonstrated efficient enrichment of HTLV-I–infected cells in the $CADM^+$ subpopulations (D and N in the CADM1 vs. CD7 plot), based on the results of real-time PCR (PVL analysis), semiquantitative PCR analysis of the *HBZ* gene, and FISH analysis (Fig. 2 and Supplementary Fig. S2). Furthermore, the CADM1 versus CD7 plot was shown to discriminate the three subpopulations more clearly than the CD3 versus CD7 plot (Fig. 1). Clonality analysis of ATLs and asymptomatic carriers (Fig. 4A and B) revealed that $CADM1^+$ subpopulations (D and N) contained

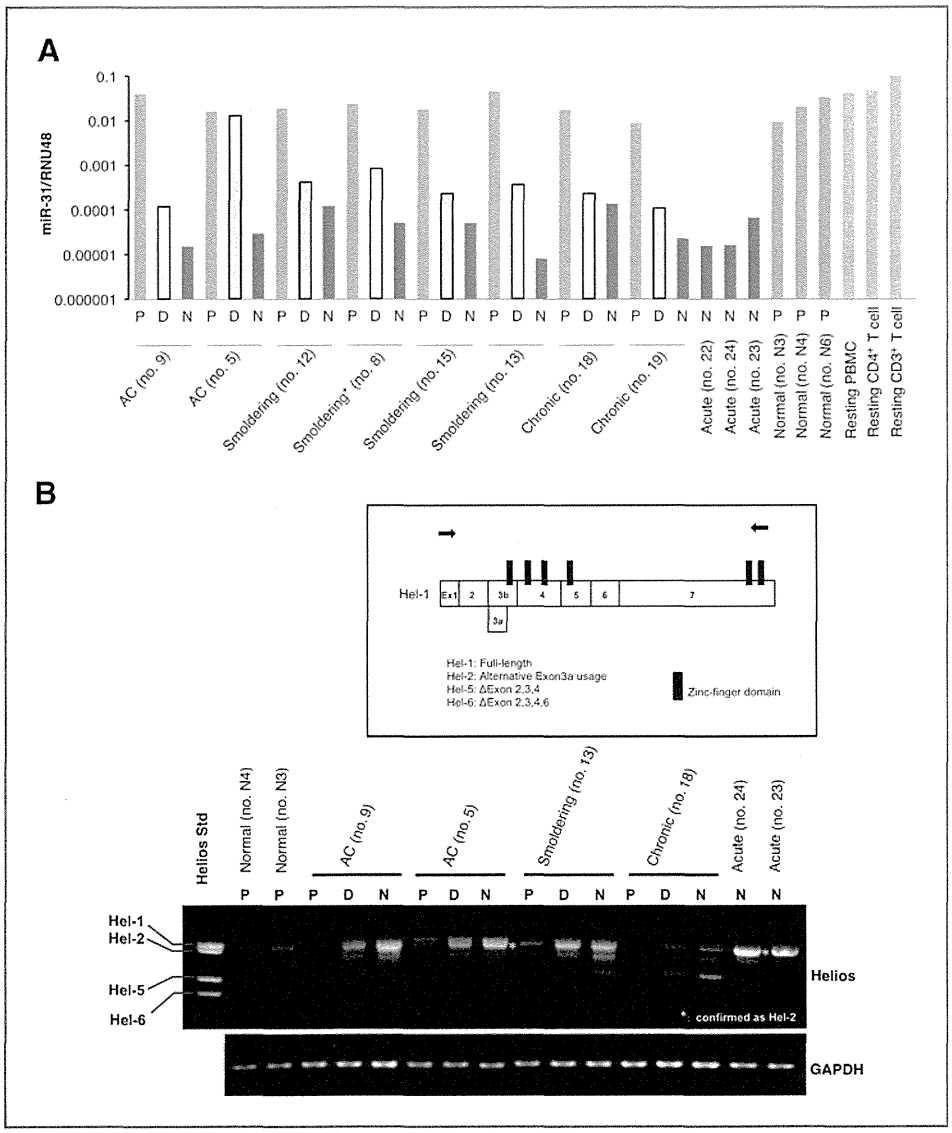

Figure 6. Gene expression pattern in the CADM1/CD7 subpopulation. A, miR-31 expression levels quantified by TaqMan-based real-time PCR. Total RNAs derived from each subpopulation were isolated and analyzed by RT-real-time PCR. RNU48 levels were also measured as an internal normalizer. *Smoldering (no. 8), this patient was considered to be at the asymptomatic carrier/smoldering borderline, because the proportion of abnormal lymphocytes fluctuated around 5%. On the day of sampling, the patient's hemogram showed 6.5% abnormal lymphocytes. B, expression analysis of *Helios* transcript variants in the subpopulations of normal controls ($n = 2$), asymptomatic carriers ($n = 2$), and ATLs (smoldering-type ATL, $n = 1$; chronic-type ATL, $n = 1$; acute-type ATL, $n = 2$). Comparisons of transcript variants among the P, D, and N subpopulations were performed by RT-PCR using primer sets specific for full-length *Helios* cDNA (top). The primer locations for *Helios* PCR are indicated by arrows in the schematic representation of *Hel-1*. The amplified cDNA (asterisk) was confirmed to be the *Hel-2* variant. The *Helios* standard (left lane), a mixture of cDNA fragments of *Hel-1*, *Hel-2*, *Hel-5*, and *Hel-6*, was used as a size indicator for each transcript variant. The glyceraldehyde-3-phosphate dehydrogenase (*gapdh*) mRNA was analyzed as an internal control (bottom).

Published OnlineFirst April 11, 2014; DOI: 10.1158/1078-0432.CCR-13-3169

clonally expanded HTLV-I–infected cells, whereas cells in the P subpopulation ($CADM1^-$) did not show clonal expansion in this analysis. Current molecular analyses of ATL cells have been limited to HTLV-I–infected cell lines and primary cells from acute/lymphoma type ATL, because in these cases, the predominant expanding clones are readily available with relatively high purity. However, the separation of clonally expanding ATL cells from indolent ATLs and asymptomatic carriers has not yet been achieved. The CADM1 versus CD7 plot from FACS allows efficient purification of such clones *in vitro*.

In an unsupervised clustering analysis of the gene expression data, the D and N subpopulations of asymptomatic carriers/indolent ATLs were grouped together, suggesting that the biologic characteristics of these subpopulations are similar (Fig. 5A and B) but distinct from the N subpopulation of acute-type ATLs (Fig. 5D). These results support the notion that in indolent ATLs and even in asymptomatic carriers, the D and N subpopulations are clonally expanding cells representing the intermediate oncogenic stage. Although the D and N subpopulations have similar gene expression profiles (Fig. 5C), there are potentially important differences distinguishing these subpopulations, according to the apparent decrease in the D subpopulation and increase in the N subpopulation that were observed as the disease progressed from indolent to acute-type ATL (Fig. 3). Detailed analysis of the genomic and epigenomic differences between these two subpopulations will provide us with information about the genomic and epigenomic lesions that are involved in disease progression. Another important finding is that the expression profiles of cells in the N subpopulation of indolent and acute-type ATLs showed significant differences, even though the majority of the genes were common to both groups (Fig. 5D). Characterization of the genes that show distinct expression patterns will reveal the molecular events that contribute to the progression from indolent to aggressive ATLs.

To address whether the emerging molecular hallmark of ATL was conserved in the novel subpopulations identified, we examined the miR-31 level and *Helios* mRNA pattern in sorted subpopulations (Fig. 6). Through integrative analyses of ATL cells, we recently showed that the expression of miR-31, which negatively regulates noncanonical NF-κB signaling by targeting NIK, is genetically and epigenetically suppressed in ATL cells, leading to persistent NF-κB activation, and is thus inversely correlated with the malignancy of the cells (31). The miR-31 levels in the P subpopulations in asymptomatic carriers and indolent ATLs were as high as those in normal P subpopulations, PBMCs, and resting T cells, whereas those in the D subpopulations decreased significantly and those in the N subpopulations were as low as in acute-type N subpopulations (Fig. 6A). Previously, we also identified ATL-specific aberrant splicing of *Helios* mRNA and demonstrated its functional involvement in ATL (32). As shown in Fig. 6B, the *Hel-2* type variant, which lacks part of exon 3 and thus lacks one of the four DNA-binding zinc-finger domains, accumulated in the D and N subpopulations of asymptomatic carriers and indolent ATLs, and was dominantly expressed in the N subpopulation of acute-type ATLs. Collectively, the molecular abnormality of ATL cells became evident in the gradual progression from P to D to N, even in asymptomatic carriers, strongly supporting the notion that the CADM1/CD7 expression pattern correlates with the multistep oncogenesis of ATL.

One of the more remarkable findings in the expression profile analysis was that the D and N subpopulations of asymptomatic carriers clustered within the same group as those of the indolent ATL cases (Fig. 5A and B). The asymptomatic carriers used in this analysis had high PVLs and relatively high proportions of the D and N subpopulations (Supplementary Table S1). In addition, mono- or oligoclonal expansion of the HTLV-I–infected cells was demonstrated in these cases. HTLV-I–infected cells in the D and N subpopulations of these asymptomatic carriers comprise clonally expanding cells that are potentially at the premalignant and intermediate stages according to their clonality, comprehensive gene expression profile, miR31 expression, and aberrant RNA splicing, all indicating that they can be categorized as asymptomatic carriers with high risk of developing into ATL, requiring careful follow-up (15, 30, 33, 34). Our flow-cytometric analysis of PBMCs from asymptomatic carriers using the CADM1 versus CD7 plot may provide a powerful tool for identifying high-risk asymptomatic carriers. Certain indolent ATL cases are difficult to distinguish from asymptomatic carriers, according to Shimoyama's criteria based on the morphologic characteristics determined by microscopic examination. Characterization of peripheral blood T cells by the CADM1 versus CD7 plot may provide useful information for clinical diagnosis.

According to Masuda and colleagues, manipulation of *CADM1* gene expression in leukemic cell lines suggested that CADM1 expression confers upon ATL cells tissue invasiveness and a growth advantage (35). The mechanism by which HTLV-I infection regulates CADM1 expression and the significance of CADM1 expression in ATL oncogenesis will require clarification by future studies.

Finally, as summarized in Supplementary Fig. S5, we demonstrated that (1) HTLV-I–infected and clonally expanded cells are efficiently enriched in $CADM1^+$ subpopulations; (2) the proportions of the three subpopulations in the CADM1 versus CD7 plot, discriminated by CADM1 expression and stepwise downregulation of CD7, accurately reflect the disease stage in HTLV-I infection; and (3) the $CADM1^+CD7^{dim/neg}$ subpopulations are at the intermediate stage of ATL progression and can be identified even in asymptomatic carriers. These findings will help to elucidate the molecular events involved in multistep oncogenesis of ATL.

Disclosure of Potential Conflicts of Interest

No potential conflicts of interest were disclosed.

Authors' Contributions

Conception and design: S. Kobayashi, T. Watanabe, K. Uchimaru
Development of methodology: T. Ishigaki, T. Yamochi, N. Watanabe

Published OnlineFirst April 11, 2014; DOI: 10.1158/1078-0432.CCR-13-3169

Acquisition of data (provided animals, acquired and managed patients, provided facilities, etc.): S. Kobayashi, E. Watanabe, K. Yuji, N. Oyaizu, S. Asanuma, A. Tojo
Analysis and interpretation of data (e.g., statistical analysis, biostatistics, computational analysis): S. Kobayashi, K. Nakano, T. Ishigaki, N. Oyaizu, M. Yamagishi, T. Watanabe
Writing, review, and/or revision of the manuscript: S. Kobayashi, K. Nakano, A. Tojo, T. Watanabe, K. Uchimaru
Administrative, technical, or material support (i.e., reporting or organizing data, constructing databases): T. Ishigaki, N. Ohno, N. Watanabe
Study supervision: A. Tojo, T. Watanabe, K. Uchimaru

Acknowledgments

The authors thank Drs. Kazunari Yamaguchi (National Institute of Infectious Diseases, Tokyo, Japan) and Yoshinori Murakami (the University of Tokyo) for their constructive comments; Yuji Zaike (Clinical Laboratory, Research Hospital, Institute of Medical Science, the University of Tokyo) for his excellent technical advice; Keisuke Takahashi, Sanae Suzuki, and members of our laboratory for assistance; and the hospital staff, which has made a commitment to providing high-quality care to all patients. The English in this document has been checked by at least two professional editors, both native speakers of English.

Grant Support

This work was supported by grants-in-aid for scientific research awarded to K. Uchimaru (no. 22591028) and T. Watanabe (no. 23390250) by the Ministry of Education, Culture, Sports, Science and Technology of Japan.

The costs of publication of this article were defrayed in part by the payment of page charges. This article must therefore be hereby marked *advertisement* in accordance with 18 U.S.C. Section 1734 solely to indicate this fact.

Received November 19, 2013; revised March 19, 2014; accepted March 26, 2014; published OnlineFirst April 11, 2014.

References

1. Yoshida M, Miyoshi I, Hinuma Y. Isolation and characterization of retrovirus from cell lines of human adult T-cell leukemia and its implication in the disease. Proc Natl Acad Sci U S A 1982;79:2031–5.
2. Osame M, Usuku K, Izumo S, Ijichi N, Amitani H, Igata A, et al. HTLV-I associated myelopathy, a new clinical entity. Lancet 1986;1:1031–2.
3. Mochizuki M, Watanabe T, Yamaguchi K, Takatsuki K, Yoshimura K, Shirao M, et al. HTLV-I uveitis: a distinct clinical entity caused by HTLV-I. Jpn J Cancer Res 1992;83:236–9.
4. Yamaguchi K, Watanabe T. Human T lymphotropic virus type-I and adult T-cell leukemia in Japan. Int J Hematol 2002;76 Suppl 2:240–5.
5. Murphy EL, Hanchard B, Figueroa JP, Gibbs WN, Lofters WS, Campbell M, et al. Modelling the risk of adult T-cell leukemia/lymphoma in persons infected with human T-lymphotropic virus type I. Int J Cancer 1989;43:250–3.
6. Iwanaga M, Watanabe T, Yamaguchi K. Adult T-cell leukemia: a review of epidemiological evidence. Front Microbiol 2012;3:322.
7. Okamoto T, Ohno Y, Tsugane S, Watanabe S, Shimoyama M, Tajima K, et al. Multi-step carcinogenesis model for adult T-cell leukemia. Jpn J Cancer Res 1989;80:191–5.
8. Matsuoka M, Jeang KT. Human T-cell leukemia virus type 1 (HTLV-1) and leukemic transformation: viral infectivity, Tax, HBZ and therapy. Oncogene 2011;30:1379–89.
9. Matsuoka M, Jeang KT. Human T-cell leukaemia virus type 1 (HTLV-1) infectivity and cellular transformation. Nat Rev Cancer 2007;7:270–80.
10. Yoshida M. Molecular approach to human leukemia: isolation and characterization of the first human retrovirus HTLV-1 and its impact on tumorigenesis in adult T-cell leukemia. Proc Jpn Acad Ser B Phys Biol Sci 2010;86:117–30.
11. Yamagishi M, Watanabe T. Molecular hallmarks of adult T cell leukemia. Front Microbiol 2012;3:334.
12. Tsukasaki K, Hermine O, Bazarbachi A, Ratner L, Ramos JC, Harrington W Jr, et al. Definition, prognostic factors, treatment, and response criteria of adult T-cell leukemia-lymphoma: a proposal from an international consensus meeting. J Clin Oncol 2009;27:453–9.
13. Ishida T, Joh T, Uike N, Yamamoto K, Utsunomiya A, Yoshida S, et al. Defucosylated anti-CCR4 monoclonal antibody (KW-0761) for relapsed adult T-cell leukemia-lymphoma: a multicenter phase II study. J Clin Oncol 2012;30:837–42.
14. Tian Y, Kobayashi S, Ohno N, Isobe M, Tsuda M, Zaike Y, et al. Leukemic T cells are specifically enriched in a unique CD3(dim) CD7(low) subpopulation of CD4(+) T cells in acute-type adult T-cell leukemia. Cancer Sci 2011;102:569–77.
15. Kobayashi S, Tian Y, Ohno N, Yuji K, Ishigaki T, Isobe M, et al. The CD3 versus CD7 Plot in Multicolor Flow Cytometry Reflects Progression of Disease Stage in Patients Infected with HTLV-I. PLoS One 2013;8:e53728.
16. Reinhold U, Abken H. CD4+ CD7- T cells: a separate subpopulation of memory T cells? J Clin Immunol 1997;17:265–71.
17. Reinhold U, Abken H, Kukel S, Moll M, Muller R, Oltermann I, et al. CD7- T cells represent a subset of normal human blood lymphocytes. J Immunol 1993;150:2081–9.
18. Leblond V, Othman TB, Blanc C, Theodorou I, Choquet S, Sutton L, et al. Expansion of CD4+CD7- T cells, a memory subset with preferential interleukin-4 production, after bone marrow transplantation. Transplantation 1997;64:1453–9.
19. Aandahl EM, Quigley MF, Moretto WJ, Moll M, Gonzalez VD, Sonnerborg A, et al. Expansion of CD7(low) and CD7(negative) CD8 T-cell effector subsets in HIV-1 infection: correlation with antigenic load and reversion by antiretroviral treatment. Blood 2004;104:3672–8.
20. Autran B, Legac E, Blanc C, Debre P. A Th0/Th2-like function of CD4+CD7- T helper cells from normal donors and HIV-infected patients. J Immunol 1995;154:1408–17.
21. Legac E, Autran B, Merle-Beral H, Katlama C, Debre P. CD4+CD7-CD57+ T cells: a new T-lymphocyte subset expanded during human immunodeficiency virus infection. Blood 1992;79:1746–53.
22. Schmidt D, Goronzy JJ, Weyand CM. CD4+ CD7- CD28- T cells are expanded in rheumatoid arthritis and are characterized by autoreactivity. J Clin Invest 1996;97:2027–37.
23. Willard-Gallo KE, Van de Keere F, Kettmann R. A specific defect in CD3 gamma-chain gene transcription results in loss of T-cell receptor/CD3 expression late after human immunodeficiency virus infection of a CD4+ T-cell line. Proc Natl Acad Sci U S A 1990;87:6713–7.
24. Sasaki H, Nishikata I, Shiraga T, Akamatsu E, Fukami T, Hidaka T, et al. Overexpression of a cell adhesion molecule, TSLC1, as a possible molecular marker for acute-type adult T-cell leukemia. Blood 2005;105:1204–13.
25. Nakahata S, Morishita K. CADM1/TSLC1 is a novel cell surface marker for adult T-cell leukemia/lymphoma. J Clin Exp Hematop 2012;52:17–22.
26. Kuramochi M, Fukuhara H, Nobukuni T, Kanbe T, Maruyama T, Ghosh HP, et al. TSLC1 is a tumor-suppressor gene in human non-small-cell lung cancer. Nat Genet 2001;27:427–30.
27. Nakahata S, Saito Y, Marutsuka K, Hidaka T, Maeda K, Hatakeyama K, et al. Clinical significance of CADM1/TSLC1/IgSF4 expression in adult T-cell leukemia/lymphoma. Leukemia 2012;26:1238–46.
28. Sugamura K, Fujii M, Kannagi M, Sakitani M, Takeuchi M, Hinuma Y. Cell surface phenotypes and expression of viral antigens of various human cell lines carrying human T-cell leukemia virus. Int J Cancer 1984;34:221–8.
29. Shimoyama M. Diagnostic criteria and classification of clinical subtypes of adult T-cell leukaemia-lymphoma. A report from the Lymphoma Study Group (1984–87). Br J Haematol 1991;79:428–37.
30. Iwanaga M, Watanabe T, Utsunomiya A, Okayama A, Uchimaru K, Koh KR, et al. Human T-cell leukemia virus type I (HTLV-1) proviral load and

Published OnlineFirst April 11, 2014; DOI: 10.1158/1078-0432.CCR-13-3169

disease progression in asymptomatic HTLV-1 carriers: a nationwide prospective study in Japan. Blood 2010;116:1211–9.

31. Yamagishi M, Nakano K, Miyake A, Yamochi T, Kagami Y, Tsutsumi A, et al. Polycomb-mediated loss of miR-31 activates NIK-dependent NF-kappaB pathway in adult T cell leukemia and other cancers. Cancer Cell 2012;21:121–35.
32. Asanuma S, Yamagishi M, Kawanami K, Nakano K, Sato-Otsubo A, Muto S, et al. Adult T-cell leukemia cells are characterized by abnormalities of Helios expression that promote T-cell growth. Cancer Sci 2013;104:1097–106.
33. Yamaguchi K, Kiyokawa T, Nakada K, Yul LS, Asou N, Ishii T, et al. Polyclonal integration of HTLV-I proviral DNA in lymphocytes from HTLV-I seropositive individuals: an intermediate state between the healthy carrier state and smouldering ATL. Br J Haematol 1988;68: 169–74.
34. Kamihira S, Iwanaga M, Doi Y, Sasaki D, Mori S, Tsurda K, et al. Heterogeneity in clonal nature in the smoldering subtype of adult T-cell leukemia: continuity from carrier status to smoldering ATL. Int J Hematol 2012;95:399–408.
35. Masuda M, Maruyama T, Ohta T, Ito A, Hayashi T, Tsukasaki K, et al. CADM1 interacts with Tiam1 and promotes invasive phenotype of human T-cell leukemia virus type I-transformed cells and adult T-cell leukemia cells. J Biol Chem 2010;285: 15511–22.

Published OnlineFirst April 11, 2014; DOI: 10.1158/1078-0432.CCR-13-3169

AACR American Association for Cancer Research

Clinical Cancer Research

CADM1 Expression and Stepwise Downregulation of CD7 Are Closely Associated with Clonal Expansion of HTLV-I–Infected Cells in Adult T-cell Leukemia/Lymphoma

Seiichiro Kobayashi, Kazumi Nakano, Eri Watanabe, et al.

Clin Cancer Res 2014;20:2851-2861. Published OnlineFirst April 11, 2014.

Cancer Science
Japanese Cancer Association JCA
Open Access

Advanced human T-cell leukemia virus type 1 carriers and early-stage indolent adult T-cell leukemia-lymphoma are indistinguishable based on CADM1 positivity in flow cytometry

Seiichiro Kobayashi,[1] Eri Watanabe,[2] Tomohiro Ishigaki,[2] Nobuhiro Ohno,[3] Koichiro Yuji,[4] Kazumi Nakano,[5] Tadanori Yamochi,[5] Nobukazu Watanabe,[2] Arinobu Tojo,[1,3] Toshiki Watanabe[5] and Kaoru Uchimaru[3]

[1]Division of Molecular Therapy, Institute of Medical Science, The University of Tokyo, Tokyo; [2]Laboratory of Diagnostic Medicine, Institute of Medical Science, The University of Tokyo, Tokyo; [3]Department of Hematology/Oncology, Research Hospital, Institute of Medical Science, The University of Tokyo, Tokyo; [4]Project Division of International Advanced Medical Research, Institute of Medical Science, The University of Tokyo, Tokyo; [5]Graduate School of Frontier Sciences, The University of Tokyo, Tokyo, Japan

Key words
Adult T-cell leukemia-lymphoma, CADM1 protein, CD7 antigen, flow cytometry, HTLV-1

Correspondence
Kaoru Uchimaru, 4-6-1 Shirokanedai, Minato-ku, Tokyo 108-8639, Japan.
Tel: 81-3-5449-5542; Fax: 81-3-5449-5429;
E-mail: uchimaru@ims.u-tokyo.ac.jp

Funding Information
Ministry of Education, Culture, Sports, Science and Technology of Japan (22591028, 23390250), Ministry of Health, Labor and Welfare of Japan (H26-sink-oujitsuyuoka-ippan-013).

Received December 15, 2014; Revised February 4, 2015; Accepted February 12, 2015

Cancer Sci (2015)

doi: 10.1111/cas.12639

We previously reported that the cell adhesion molecule 1 (CADM1) versus CD7 plot in flow cytometry reflects disease progression in human T-cell leukemia virus type 1 (HTLV-1) infection. In $CD4^+$ cells from peripheral blood, $CADM1^-CD7^+$ (P), $CADM1^+CD7^{dim}$ (D) and $CADM1^+CD7^-$ (N) subpopulations are observed. The D and N subpopulations increase as asymptomatic HTLV-1 carriers (AC) progress to indolent adult T-cell leukemia-lymphoma (ATL) and the N subpopulation then expands in aggressive ATL. In the present study we examined whether the analysis can estimate the risk of developing ATL in advanced AC. Peripheral blood samples from AC ($N = 41$) and indolent ATL patients ($N = 19$) were analyzed by flow cytometry using the CADM1 versus CD7 plot for $CD4^+$ cells and inverse long PCR (clonality analysis) of FACS-sorted subpopulations. Almost all AC with a high HTLV-1 proviral load (>4 copies/100 cells) had a $CADM1^+$ (D + N) frequency of >10%. AC with 25% < $CADM1^+ \leq 50\%$ contained expanded clones similar to smoldering-type ATL. In many patients in the 25% < $CADM1^+ \leq 50\%$ group, the proportion of abnormal lymphocytes was distributed around the 5% line, which divides AC and smoldering-type ATL in Shimoyama's classification. In conclusion, the CADM1 versus CD7 plot is useful for selection of putative high-risk AC. The characteristics of some AC and smoldering ATL are said to be similar; however, long-term follow up is required and the clinical outcome (e.g. rate of transformation) of these cases should be used to determine whether to include them in the same clinical category.

Human T-cell leukemia virus type 1 (HTLV-1) is a human retrovirus that causes HTLV-1–associated diseases such as adult T-cell leukemia-lymphoma (ATL, a neoplastic disease of $CD4^+$ T cells), HTLV-1-associated myelopathy/tropical spastic paraparesis (HAM, a chronic inflammatory disease of the central nervous system) and HTLV-1 uveitis (HU, a subacute inflammatory disease of the uvea).[1–3] A recent report estimated that 5–10 million people are HTLV-1-infected worldwide.[4] In Japan, the estimated lifetime risk of developing ATL in HTLV-1 asymptomatic carriers (AC) is 6–7% for males and 2–3% for females.[5–7]

We recently developed a flow cytometry-based method that enables HTLV-1-infected and clonally expanding cells to be purified.[8–10] In the cell adhesion molecule 1 (CADM1) versus CD7 plot for $CD4^+$ cells in peripheral blood mononuclear cells (PBMC) from HTLV-1-infected patients, three subpopulations (P, $CADM1^-CD7^+$; D, $CADM1^+CD7^{dim}$; and N, $CADM1^+CD7^-$) are consistently observed.[10] HTLV-1-infected cell clones are enriched in the $CADM1^+$ subpopulations (D and N). In the early stage of ATL development (from AC to indolent ATL), the D and N subpopulations increase concomitantly with clonal growth of these subpopulations. In the late stage (from indolent ATL to aggressive ATL), the N subpopulation expands, indicating loss of CD7 in the $CADM1^+$ subpopulations. Therefore, the CADM1 versus CD7 profile enables objective evaluation of HTLV-1 disease progression regardless of the disease stage in HTLV-1 infection.

Factors associated with development of ATL have been reported to include HTLV-1 infection through breastfeeding, advanced age and family history of ATL.[7,11] A recent epidemiological study in Japan revealed that AC with a high proviral load (PVL, more than four copies per 100 PBMC) are at high risk of developing ATL.[12] Other definitive risk factors for the development of ATL have not been determined.

In this study we propose that our flow cytometry (CADM1 versus CD7 plot) will help to identify high-risk AC. The flow cytometric profiles of AC varied widely, with some AC having increased $CADM1^+$ subpopulations to the same degree

as indolent ATL. These AC were indistinct from early-stage indolent ATL based on the CADM1 versus CD7 profile, clonality analysis and clinical data (PVL and percentage of abnormal lymphocytes). Our flow cytometric analysis revealed that some AC and smoldering ATL have similar characteristics, indicating the need for careful clinical follow up of these cases and that flow cytometry can be used to identify putative high-risk AC.

Materials and Methods

Cell lines and patient samples. TL-Om1, an HTLV-1-infected cell line, was provided by Dr Sugamura (Tohoku University, Sendai, Japan). Peripheral blood samples were collected from inpatients and outpatients at our hospital from June 2011 to September 2014, as described in our previous reports.[8–10] As shown in Table 1, 60 cases were analyzed (41 AC; 9 cases of smoldering-type ATL; 10 cases of chronic-type ATL). All patients with ATL were categorized into clinical subtypes according to Shimoyama's criteria.[13,14] Patients with various complications, such as autoimmune disorders and systemic infections, were excluded. The present study was approved by the Institutional Review Board of our institute (University of Tokyo). Written informed consent was obtained from all patients.

Flow cytometry and cell sorting. Peripheral blood mononuclear cells were isolated from whole blood by density gradient centrifugation, as described previously.[8] An unlabeled CADM1 antibody (clone 3E1) and an isotype control chicken IgY antibody were purchased from MBL (Nagoya, Japan). These were biotinylated (by primary amine biotinylation) using biotin *N*-hydroxysuccinimide ester (Sigma Aldrich, St. Louis, MO, USA). A Pacific Orange-conjugated anti-CD14 antibody was purchased from Life Technologies (Carlsbad, CA, USA). All other antibodies were obtained from BioLegend (San Diego, CA, USA). Cells were stained using a combination of biotin-CADM1, allophycocyanin (APC)-CD7, APC-Cy7-CD3, Pacific Blue-CD4 and Pacific Orange-CD14. After washing, phycoerythrin (PE)-conjugated streptavidin was applied. Propidium iodide (PI [Sigma Aldrich]) was added to the samples to stain dead cells immediately before flow cytometry. A FACSAria instrument (BD Immunocytometry Systems, San Jose, CA, USA) was used for all multicolor flow cytometry and fluorescence-activated cell sorting (FACS). Data were analyzed using the FlowJo software (TreeStar, San Carlos, CA, USA). The gating procedure was as described previously.[10] Briefly, PI^+ cells and then $CD14^+$ cells were gated out. Next, a CADM1 versus CD7 plot for $CD4^+$ cells was constructed (Fig. 1a).

Quantification of human T-cell leukemia virus type 1 proviral load by real-time quantitative PCR. Proviral load in FACS-sorted PBMC was quantified by real-time quantitative PCR (TaqMan method) using the ABI Prism 7000 sequence detection system (Applied Biosystems, Foster City, CA, USA), as described previously.[8,12]

Inverse long PCR to assess the clonality of human T-cell leukemia virus type 1-infected cells. For clonality analysis, inverse long PCR was performed as described previously.[8] First, 1 μg of genomic DNA extracted from FACS-sorted cells was digested with PstI at 37°C overnight. RNase A (Qiagen, Hilden, Germany) was added to remove residual RNA completely. DNA fragments were purified using a QIAEX2 gel extraction kit (Qiagen). The purified DNA was self-ligated with T4 DNA ligase (Takara Bio, Otsu, Japan) at 16°C overnight. Inverse long PCR was performed using Tks Gflex DNA Polymerase (Takara Bio). The forward primer was 5′-CAGCCCATTCTATAGCACTCT CCAGGAGAG-3′ and the reverse primer was 5′-CAGTCTCC AAACACGTAGACTGGGTATCCG-3′. Processed genomic DNA (50 ng) was used as the template. The reaction mixture was subjected to 35 cycles of denaturation (94°C, 30 s) and annealing plus extension (68°C, 8 min). The PCR products were subjected to electrophoresis on 0.8% agarose gels. For samples from which a sufficient amount of DNA was extracted, PCR was generally performed in duplicate.

Statistical analyses. Statistical comparisons were performed by Kruskal–Wallis non-parametric ANOVA and Dunn's procedure for pairwise comparisons using GraphPad Prism version 5.0a (GraphPad Software, San Diego, CA, USA). $P < 0.05$ was taken to indicate statistical significance.

Results

Asymptomatic carriers with high proviral load have increased $CADM1^+$ subpopulations. Because high PVL (more than four copies per 100 PBMC) is one of the major risk factors for AC to develop ATL,[12] we first analyzed the relationship between the CADM1 versus CD7 profile and PVL. A representative CADM1 versus CD7 profile is shown in Figure 1(a). As shown in Figure 1(b), almost all AC with high PVL had $CADM1^+$ (D + N) subpopulations of >10% (24 of 25 cases). Conversely, AC with a $CADM1^+$ population of ≤10% predominate in those with a PVL of fewer than four copies per 100 PBMC (15 of 16 cases). In this study, $CADM1^+$ (%) indicates the proportion of $CD4^+$ cells that were $CADM1^+$ unless otherwise stated. PVL indicates the number of HTLV-1 copies/100 PBMC (HTLV-1-infected T cells generally contain a single integrated provirus).[15] To compare both factors directly, the $CADM1^+$ (%) for PBMC was calculated by taking the percentage of $CD4^+$ cells and all lymphocytes into account. As shown in Figure S1, the $CADM1^+$ (%) for PBMC was nearly equal to the PVL in AC.

Clonality analysis of $CADM1^+$ subpopulations in asymptomatic carriers and indolent ATL. The three subpopulations (P, D and N) in the CADM1 versus CD7 plot were FACS-sorted and subjected to clonality analysis (by inverse long PCR).

Table 1. Clinical profile of HTLV-1 infected patients in the present study

Clinical subtype	Number of cases	Male	Female	Age (range)	WBC (per μL) (range)	Lymphocytes (%) (range)	Abnormal lymphocytes (%) (range)
HTLV-1 AC	41	14	27	52.8 (31–69)	5694 (3110–10360)	33.0 (17.5–44.5)	1.9 (0.0–4.7)
Smoldering	9	3	6	56.0 (43–72)	5561 (2620–7270)	29.9 (11.0–39.5)	9.3 (5.0–24.5)
Chronic	10	5	5	54.3 (43–67)	12345 (7780–25570)	31.6 (5.5–64.0)	32.1 (6.0–60.5)

Average of age, WBC, lymphocytes (%) and abnormal lymphocytes (%) are shown. Proportion of abnormal lymphocytes in the peripheral blood WBC were evaluated by morphological examination. AC, asymptomatic carrier; HTLV-1, human T-cell leukemia virus type 1; WBC, white blood cells (normal range, 3500–9100/μL).